DEVELOPMENT OF MULTI-ELEMENT ACTIVE AERODYNAMICS

FOR THE FORMULA SAE CAR

by

JAMES PATRICK MERKEL

Presented to the Faculty of the Graduate School of

The University of Texas at Arlington in Partial Fulfillment

of the Requirements

for the Degree of

MASTER OF SCIENCE IN AEROSPACE ENGINEERING

THE UNIVERSITY OF TEXAS AT ARLINGTON

December 2013

Abstract

DEVELOPMENT OF MULTI-ELEMENT ACTIVE AERODYNAMICS

FOR THE FORMULA SAE CAR

James Merkel

The University of Texas at Arlington, 2013

Supervising Professor: Robert L. Woods

This thesis focuses on the design, development, and implementation of an active aerodynamics system on 2013 Formula SAE car. The aerodynamics package itself consists of five element front and rear wings as well as an under body diffuser. Five element wings produce significant amounts of drag which is a compromise between the cornering ability of the car and the acceleration capability on straights. The active aerodynamics system allows for the wing angle of attack to dynamically change their configuration on track based on sensory data to optimize the wings for any given scenario. The wings are studied using computational fluid dynamics both in their maximum lift configuration as well as a minimum drag configuration. A control system is then developed using an electro mechanical actuation system to articulate the wings between these two states.

TABLE OF CONTENTS

List of Illustrations

List of Tables

Chapter 1

Introduction

Vehicle aerodynamics is a broad encompassing field that describes the forces acting on an object when moving through a fluid. When stationary, the exterior surfaces of an automobile experience one atmospheric pressure; the upper and lower surface as well as the front and rear surfaces all have the same pressures exerted and ultimately achieve equilibrium with the summation of forces being equal to zero. As the vehicle starts to move through the fluid, the pressures exerted on the exterior surfaces change proportional to the square of velocity. These pressure changes create forces acting on the surface of the vehicle that can drastically hinder the performance of the vehicle. Aerodynamicists study this natural phenomenon to try and minimize forces that inhibit motion and in some cases, develop these forces and use them to improve performance and safety.

1.1 Vehicle Aerodynamics

Vehicle aerodynamicists are primarily concerned with two dominant forces that interact with a vehicle; lift and drag. These forces and the standard coordinate system for a vehicle are shown in figure 1.
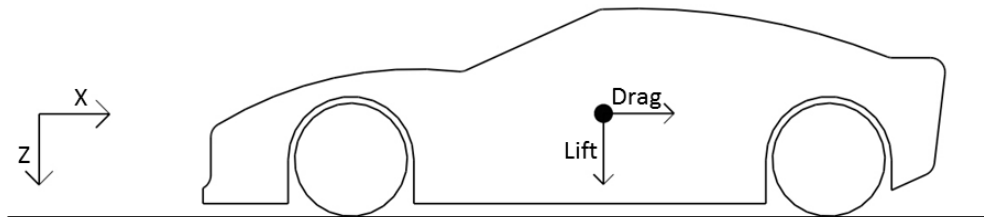
Figure 1. Downforce and drag forces and applicable coordinate system.

The lifting force is resolved along the Z-axis. Nomenclature follows the convention that the lift vector in the negative Z-direction is known purely as lift; this vector in the opposite direction is downforce. The drag force is resolved along the Y-axis with

the vector in the positive direction known as drag. The opposite of drag, is considered thrust, this force is not usually found in traditional vehicle aerodynamics.

The management of these forces is crucial to the performance of any vehicle however the philosophy of vehicle aerodynamics differ significantly depending on the application. For instance the automotive and transportation industries seek to minimize the drag force to improve fuel economy at highway speeds. The aviation industry seeks to maximize the overall efficiency or lift divided by drag of their vehicles. The more lift produced, the larger loads the aircraft can carry and the smaller drag force allows for better fuel consumption.

1.2 Race industry

Depending on the rules of the series, the race industry has different criteria for the development of their vehicle aerodynamic. Although the aerodynamic design philosophies may differ based on rules and regulations, in general, engineers seek to maximize negative lift or down force within some allowable drag limit which is determined by a combination of top speed and fuel requirements. Increasing the downforce on the car increases the normal load on the tires which translates to an increase in overall cornering grip and likewise overall performance and reduction in lap time.

Joseph Katz comments that, "aerodynamic downforce has only recently been understood and used efficiently in the past 40 years" [7]. Figure 2 shows the increase in the lap speed record at the Indianapolis Motor Speedway. The first aerodynamic devices used for racing applications occurred around 1960 where the trend first starts to increase sharply. He also notes that around 1970 was the first efficiently designed aerodynamics package for a racing application which resulted in another large increase in lap speed [7].
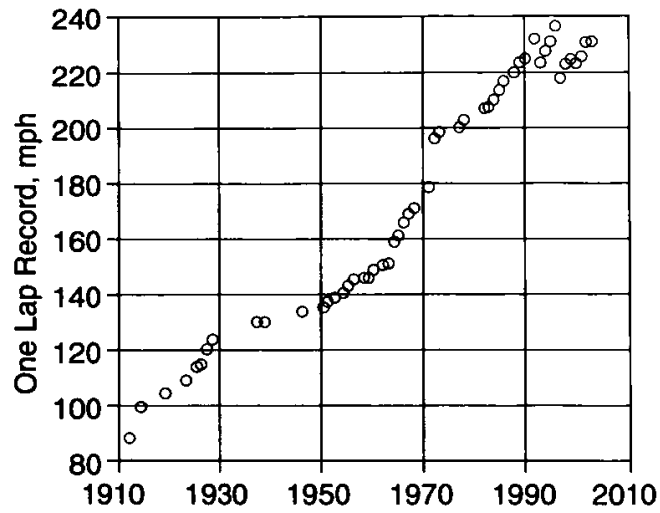
Figure 2. Variation of one lap record speed at Indianapolis Motor Speedway [7].

1.3 Aerodynamic Devices

The most common and obvious aerodynamic devices used in racing include a front and rear wing, and underbody diffuser. The racing series regulations dictate how these components are sized and their general placement. These devices are shown in figure 3 on the 2012 UTA Formula SAE (FSAE) Car.
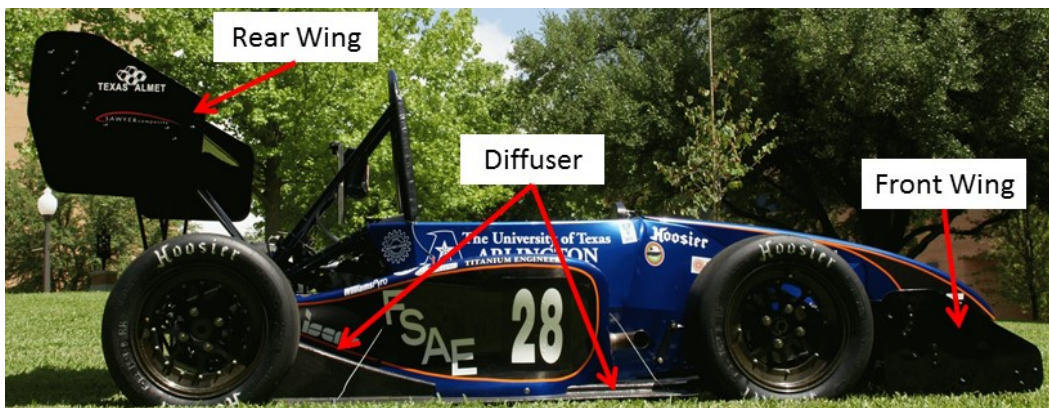
Figure 3. UTA F12 Formula SAE Car with front and rear wing as well as diffuser.

1.3.1 Front Wing

The front wing is designed to produce enormous amounts of downforce while operating in ground effect and typically uses either a single or multi-element design depending on the rules. Endplates are used to minimize tip losses and can vary in size, shape, and complexity. This aerodynamic device is the most important design feature of any vehicle because it sets up the airflow for the entire rear of the vehicle as well as dictates the size and placement of the rear wing to properly balance a car aerodynamically. Since the front wing is the first object to disturb flow around the vehicle, a poorly designed front wing can result in very large drag increases and losses across the entire rear of the car.

1.3.2 Diffuser

The underbody diffuser seeks to utilize the underbody of the car to produce downforce. Similar to the front wing it too operates in ground effect. The design of an under tray can utilize tunnels, stepped underbody, or just a flat surface with a diffuser section at the rear of the car to lower the pressure underneath the car. Diffusers will have a lower lift coefficient than the front and rear wing however due to the large amount of wetted area underneath the car, properly designed diffusers are the most efficient at generating downforce.

1.3.3 Rear Wing

The rear wing is designed to complement the downforce levels and aerodynamic balance of the front wing and diffuser. Similar to front wings, a rear wing can use either a single or multi element layout with large endplates to mitigate tip losses.

1.4 Formula SAE

The Formula SAE is the premier collegiate design series sponsored and hosted by the SAE International that gives students the opportunity to get hands-on real world

experience while designing, building, and testing an open wheel formula style race car to be marketed to a weekend autocrosser. Each year, hundreds of team around the world start development of new cars and have the opportunity to compete at nine different international competitions around the world. Each competition is broken up into static and dynamic events. The static events consist of cost analysis of the car, business and marketing presentation, and a design event. Dynamic events consist of a drag race to gauge the acceleration of the cars, skid pad which measures the handling of the cars, autocross which gauges the ability of the car to maneuver on course without other vehicles in the way, and an endurance race which consists of a 22 km autocross race with a driver change in the middle [5]

1.4.1 Autocross

Autocross is a unique form of racing where different tracks are setup using traffic cones in open parking lots and other large paved surface venues. The style of racing is against the clock rather than wheel to wheel to ensure the safety of the drivers while also putting emphasis purely on driver skill and car setup. Drivers compete on a new course for every event and will never see the same course twice.

At the start of race day, the new course is opened for walking allowing the drivers to get their first look at the new track and study its layout. The task at hand is to read the course and determine the appropriate driving line based on the limits of the vehicle. Racers then have the opportunity to drive the course at full speed with no practice and typically have three to five chances to get the fastest time before never seeing the course again.

With this style of racing autocross times are recorded down to the millisecond and races are frequently won and lost by milliseconds with the top places at an event typically being separated by only a few hundred milliseconds. In fact, UTA holds the

record for the smallest margin of victory able to be recorded winning the 2010 SCCA

Nationals event by .001 seconds.

1.4.2 Competition Description

As with any racing series, SAE international publishes an updated rule book that

the cars must adhere to as well as dictating the structure of each event. However FSAE

is unique in that it allows for the most design freedom of any racing series. The 2013

Formula SAE Rules quote the competition objective as:

> "A1.1.1 To give teams the maximum design flexibility and the freedom to
> express their creativity and imaginations there are very few restrictions
> on the overall vehicle design. The challenge to teams is to develop a
> vehicle that can successfully compete in all the events described in the
> FSAE Rules. The competitions themselves give teams the chance to
> demonstrate and prove both their creativity and their engineering skills in
> comparison to teams from other universities around the world." [5].

1.4.3 Aerodynamic Rules

Since the rules regulating the design of Formula SAE cars are fairly broad, there

is fairly little constraint on any aerodynamic devices. In fact, with the 2011 revisions to the

rulebook, the regulations were relaxed further prompting massive aerodynamic

development amongst the teams. The current FSAE rules for aerodynamics are as

follows:

> T9.2 Location - In plain view, no part of any aerodynamic device, wing,
> under tray or splitter can be:
> a. Further forward than 762 mm (30 inches) forward of the fronts of the
> front tires
> b. No further rearward than 305 mm (12 inches) rearward of the rear of
> the rear tires.
> c. No wider than the outside of the front tires or rear tires measured at
> the height of the hubs, whichever is wider.
> T9.3 Minimum Radii of Edges of Aerodynamic Devices - All wing edges
> including wings, end plates, Gurney flaps, wicker bills and undertrays
> that could contact a pedestrian must have a minimum radius of 1.5 mm
> (0.060 inch)

T9.4 Ground Effect Devices – no power device may be used to move or remove air from under the vehicle except fans designed exclusively for cooling. Power ground effects are prohibited [5].

1.5 Active Aerodynamics

Active aerodynamics is a field that relatively little development has taken place in. Conceptually, active aerodynamics would consist of any type of movable surfaces or wing elements that change their position based on some input whether it's from a driver an independent controller. Using a driver input will limit controls to two states or positions. True active aerodynamics requires an electronics system that takes sensory input and adjusts aerodynamic surfaces dynamically to optimize the aerodynamics for a given condition.

1.5.1 Movable Aerodynamics for Racing

The first car to officially be raced with wing elements installed is credited to Chaparral Cars Inc. In 1966, its iconic high mount single element rear wing was controlled by a foot petal in the driver's compartment. When cornering, the wing would pitch down providing downforce and thus higher cornering speed. However the driver could pitch the wing up in a straight line to minimize drag thus achieving higher speed on the straights than any of its competitors [10]. However wing failures resulted in stronger regulation in Can-Am, Formula 1, and other racing series that outlawed wings moving relative to the chassis. The Chaparral 2E car is shown in figure 4.

Figure 4. Chaparral 2E racecar with driver controlled rear wing [3].

Regulations have evolved in Formula 1 today to allow a Drag Reduction System (DRS) on the rear of the car to increase passing. It consists of a movable flap on the rear of the car that is activated by the driver to stall the main plane and achieve higher top speeds. The use of it though is limited to certain parts of the track and only when following another car.

1.5.2 Active Aero in Street Vehicles

Active aerodynamics has started making its debut into the consumer market both to increase fuel efficiency, high speed stability, and track performance. Car manufacturers that have started incorporating active aerodynamics involve vehicles range from exotic sports car manufacturers such as Pagani, Ferrari, and McLaren to more mass produced vehicles from manufactures such as the Ford, Volkswagen, and many others.

1.6 Objective of Thesis

The objective of this thesis is to develop and implement a multi-element active aerodynamics system to be used on the 2013 FSAE car. The fully-functional system will require aerodynamic, mechanical, and electrical analysis and design. The complete

system will consist of the aerodynamic analysis to understand the forces acting on each individual wing element as well as the control system to actuate the elements. Development of the control scheme and hardware will be done in conjunction with an embedded electronics engineer to design the circuit and software needed to control the wings. This platform can then be used to develop more advanced control schemes for future work.

1.7 Outline of Thesis

This thesis is broken down into nine chapters. Because of the multidisciplinary nature of developing a complete active aerodynamics system, each chapter will discuss one aspect of the design process.

Chapter 1 discusses the different types of aerodynamic devices used on race cars and their importance to improving lap times. It also discusses the competition and rules governing aerodynamics in Formula SAE.

Chapter 2 details the process of choosing a multi-element wing platform to develop into an actively controlled wing. It also calculates the predicted gains of an active aerodynamics system both in straight line acceleration and lap time reduction.

Chapter 3 talks about the aerodynamic analysis of the five-element wing and calculating the torques required to rotate each flap individually.

Chapter 4 discusses the philosophy, initial design, and control schemes used by the active aerodynamic system which dictate its behavior on track. This will influence the design of the system both physically and ultimately dictate the electronics architecture.

Chapter 5 discusses the actuation mechanism and how the flaps are controlled by the servos. The linkage design parameters are discussed as well as the analysis procedure to design the flap control system.

Chapter 6 details the servo motor selection and electronic packaging for the wings. It also discusses the software controls used for the wings and tuning of the wing to change wing behavior.

Chapter 7 analyses the wing from an aeroelastic perspective. It details the procedure used to calculate the time for airflow to reattach on the wing when moving from an open to a closed state.

Chapter 8 briefly shows the build process, system components, and total weight as well as photos of the completed wings.

Chapter 9 talks about the conclusions from the design work on the 2013 FSAE car and areas of future work.

The appendices give more details of various topics discussed in the thesis.

Chapter 2

Conceptual Performance and Sizing

2.1 Introduction

Both four and five-element wing designs were considered for the 2013 Formula SAE car. Each wing package is studied using an in-house lap simulation tool for both a static and active wing configurations to determine the benefits of one wing design over another. The basis for the comparison is data taken from 2D simulations. The simulation data is corrected to approximate 3D effects which is then used in the lap simulation tool. The track used for simulation is the 2012 FSAE Lincoln autocross course. The performance gains between an active and non-active wing are also investigated such as top speed and vehicle acceleration.

2.2 Simulation Data for Four and Five-Element Wing Profiles

The wing element design consists of a leading edge slat, a main plane and the respective number of flaps. The different parts of a multi-element wing are shown in figure 5.
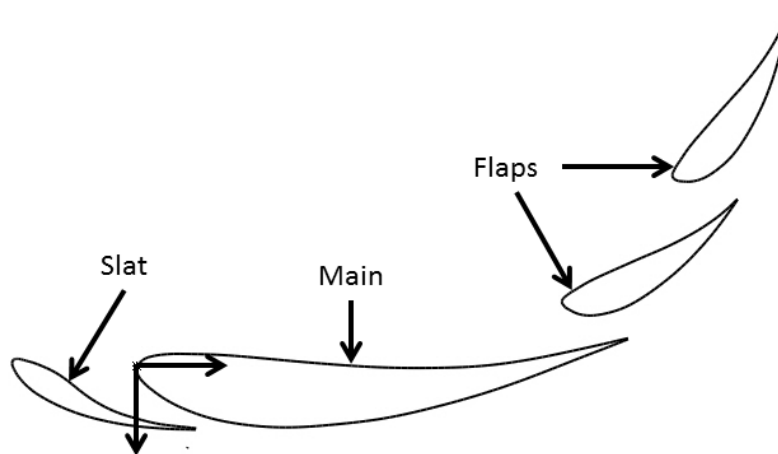
Figure 5. Multi-element Wing.

The simulation data is calculated using computational fluid dynamics (CFD). The meshes are generated using Pointwise, which is standalone mesh generation software allowing for very fine control over all parts of the mesh and can build grids very quickly. These grids are uploaded into StarCCM+ which is the CFD solver.

2.2.1 2D Simulation Data

The multi-element wings were designed in 2D using a UTA developed genetic algorithm that created a closed-loop process integrating Pointwise and StarCCM+. The code generated potential solutions and simulated each iteration while monitoring the lift coefficient. The code will then iterate the wing element placement searching for their optimum location to maximize the lift coefficient. This process is presented by Aaron one in reference [8]. This streamlined the wing design process. The user uploads the slat, main, and respective number of flaps and allowing the computer to iterate until the wing converged on a placement solution. The process diagram can be seen below.
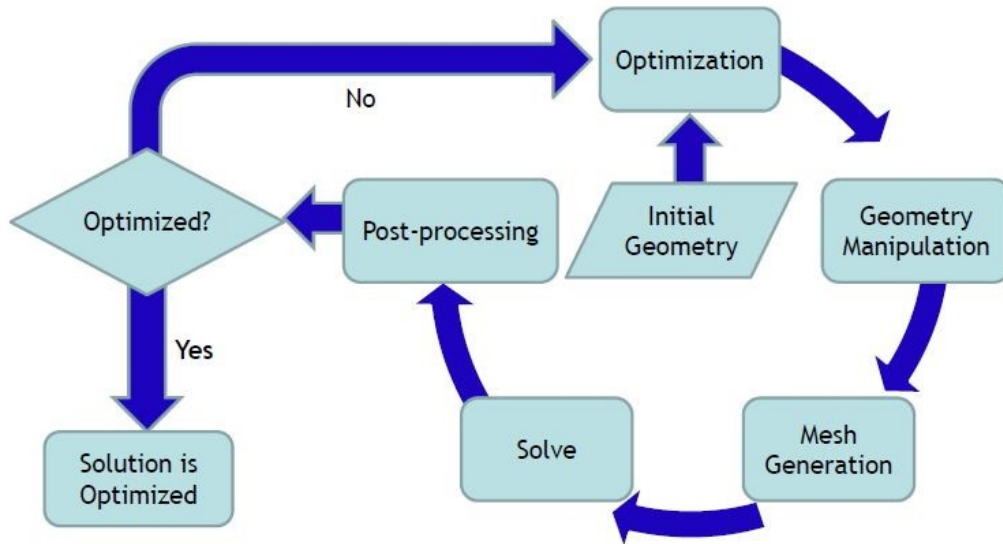
Figure 6. Optimization algorithm process [8].

Once the wing placement is complete for both the four and five-element wing, the flaps are rotated about their quarter-cord point for minimum drag. This is considered the open-wing state. Both closed and open-wing states can be seen in figure 7.

Figure 7. Multi-element wing in closed and open-position.

For each simulation lift and drag are monitored for convergence. The moment taken about the origin of the main plane is also monitored for each element. The 2D values for these data sets are given below for both the four and five-element wing. The wings are simulated at a free-stream speed of 30 mph or 13.4 m/s and standard atmospheric conditions.

Table 1. 2D Simulation Data.

4 Element Wing

2D CFD Data Closed	[SI]		[US]	
2D Lift: L =	181.7	[N]	40.9	[lbf]
2D Drag: D =	10.8	[N]	2.4	[lbf]
2D Moment: M =	-23.9	[N-m]	-211.8	[lbf-in]

2D CFD Data Open	[SI]		[US]	
2D Lift: L =	52.2	[N]	11.7	[lbf]
2D Drag: D =	0.5	[N]	0.1	[lbf]
2D Moment: M =	6.5	[N-m]	57.5	[lbf-in]

5 Element Wing

2D CFD Data Closed	[SI]		[US]	
2D Lift: L =	258.1	[N]	58.0	[lbf]
2D Drag: D =	19.3	[N]	4.3	[lbf]
2D Moment: M =	-40.7	[N-m]	-360.3	[lbf-in]

2D CFD Data Open	[SI]		[US]	
2D Lift: L =	107.5	[N]	24.2	[lbf]
2D Drag: D =	4.8	[N]	1.1	[lbf]
2D Moment: M =	-19.7	[N-m]	-174.5	[lbf-in]

2.2.2 Correction for 3D effects in free-stream

Lift and drag coefficients are calculated from the data shown in table 1. The drag coefficient is corrected for induced drag since only viscous drag is accounted for in a 2D simulation. Also correction factors for endplate effects are applied to approximate 3D effects. This data is then used to model the car with different aerodynamic packages in the lap simulation tool. The procedure to approximate 3D effects is given in Appendix A.

The corrected 3D lift and drag values for the rear wing are shown in the table 2. Both the four and five-element wing is shown as well as the open and closed-state. Table 3 gives the corrected values for the front wing.

Table 2. 3D lift and drag coefficients for the rear wing.

3D Rear Closed	4E	5E
Drag Coefficient: C_D =	1.10	1.56
Lift Coefficient: C_L =	3.67	4.27
3D Rear Open		
Drag Coefficient: C_D =	0.08	0.30
Lift Coefficient: C_L =	1.05	1.78

Table 3. 3D lift and drag coefficients for the front wing.

3D Front Closed	4E	5E
Drag Coefficient: C_D =	1.15	1.51
Lift Coefficient: C_L =	4.77	6.40
3D Front Open		
Drag Coefficient: C_D =	0.09	0.29
Lift Coefficient: C_L =	1.37	2.67

2.3 Lap simulations

In 2012 team member Siddarth Kashyap developed a Matlab based lap simulation tool that predicts lap times for each of the four dynamic events at the Formula SAE competition. The simulation tool takes into account various vehicle parameters such as wheelbase, track, vehicle weight, and CG height as well as engine maps and aerodynamic data from the car and makes lap predictions based on a car with an ideal driver [2]. Although the simulation tool gives an idealized case it can make adequate predictions on performance trends by varying different parameters; in this case, the aerodynamics package.

2.3.1 Lap Simulation Setup

The AeroMap module accounts for lift and drag coefficients of each aerodynamic device individually including that of the car without aerodynamic devices. After inputting all the wing data, the global lift and drag coefficients of the car are calculated based on the frontal area of the vehicle. The aerodynamic balance of the car is calculated based on wing placements. These final values are used in the actual lap simulation.

For each scenario, the aerodynamic balance of the car is assumed to be 52% of the wheelbase. This ensures that the only variable affecting lap times is the global vehicle force coefficients. Since the actual wing placement is not yet known, this correction was made by adjusting the center of pressure of the vehicle given by the "Xcp" input of the

15

vehicle information box until the target aero distribution is met. The interface for inputting aerodynamic data is shown in figure 44 in Appendix B.

2.3.2 Track Map Used for Simulation

The competition organizers have released site maps of the competition that give course data for both autocross and endurance. These maps give corner radiuses as well as spacing between certain gates and slaloms. The latest course data available is 2012 FSAE Lincoln autocross course shown in figure 8. Since the 2013 tracks are not released until a month before the competition, this course is used for simulation purposes.
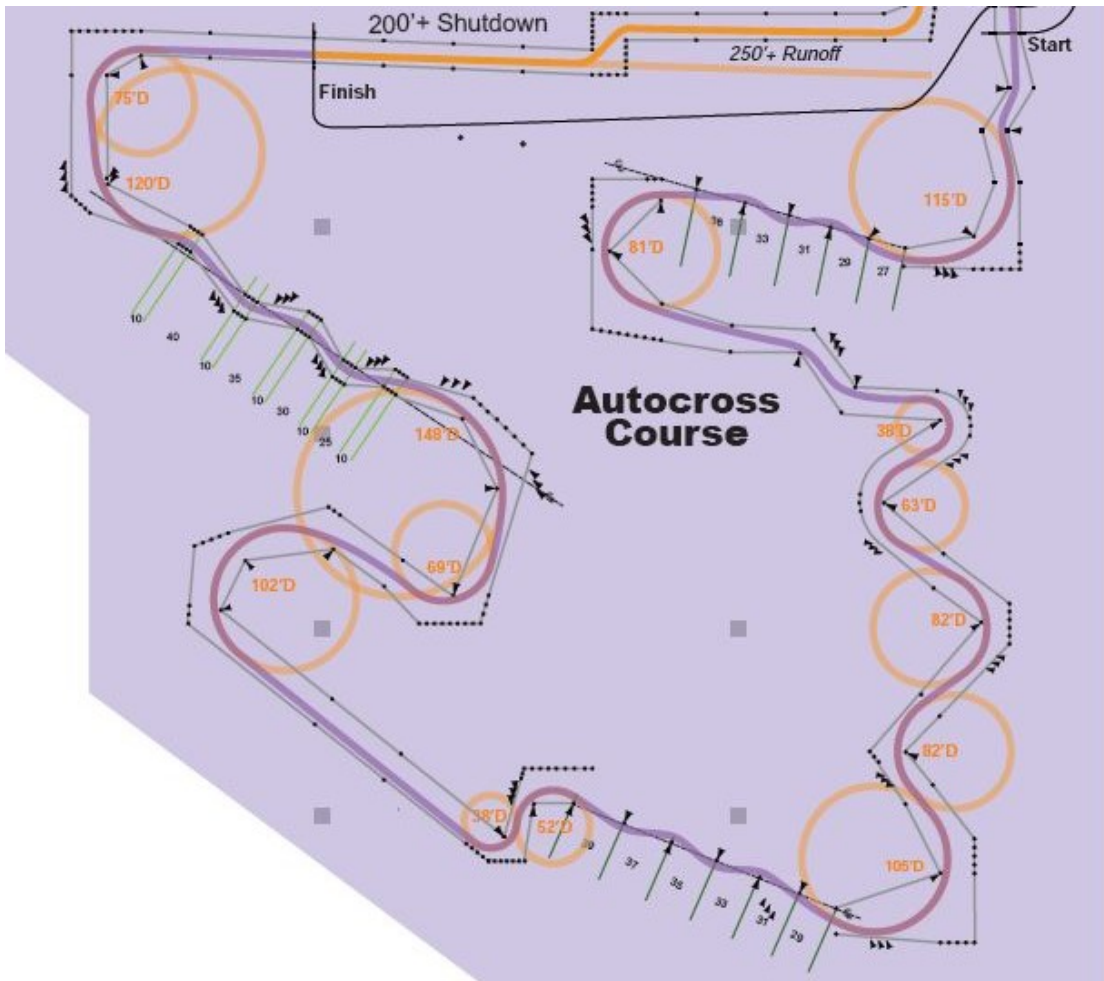
Figure 8. 2012 FSAE Lincoln autocross course.

2.3.3 Lap Simulation Process

Five different case scenarios are performed in the lap simulator; no aero, four and five-element static, as well as four and five-element active wings. The solver operates via an iterative process to calculate maximum cornering *g's* as well as acceleration and deceleration *g's* by breaking up the track into a series of straights and corners [2]. This means that straight line performance is a function of the global vehicle drag coefficient only and the cornering performance is a function of both the vehicle lift coefficient and aerodynamic balance. This decoupling of lift and drag in the simulation means that calculating lap times with active aerodynamics is simply using the drag coefficient for the open-wing while maintain the aerodynamic balance of the car. The report *Lap Simulation and Path Optimization* describes the iterative process in more detail. It is summed into a four step process.

1. Solve for maximum velocities through corners and slaloms

2. Calculate straight line speed into first corner

3. Compare speed at end of the straight to maximum cornering velocity

   a. For a straight line speed greater than cornering speed, calculate braking requires.

   b. For a straight line speed less than cornering speed, solve for the corner with the slower velocity.

4. Iterate through each combination of straight and corner for the rest of the track [2]

All other vehicle parameters were set to those of the 2013 car. The input window is shown below in the next figure. These values were held constant for each vehicle simulation. The engine model selected was that of a stock YZF 450 from the engine selection menu.

Figure 9. Lap simulator car map window with default parameters for the 2013 car.

The aerodynamic balance of the car is held constant to achieve a 52% rearward balance. This equates to 32.76" aft of the front tire contact patch and a static margin of 0 for the vehicle. In each case this was accomplished by adjusting the center of pressure of the vehicle. The lift and drag coefficients as well as the center of pressure of the vehicle itself are calculated based on wind tunnel data of the vehicle itself without any aerodynamic devices from previous years [1].

The aerodynamic parameters are the only variation made to the lap simulator to ensure a direct comparison between aero packages. The inputs are made in the aero map module shown in figure 44. The aerodynamic data used for each case is shown in table 4.

Table 4. Aerodynamic data input into the lap simulation tool.

Case	Wing	State	Front Wing		Rear Wing		Vehicle (Calculated From Sim.)		
			Cl	Cd	Cl	Cd	Cl	Cd	Cp [in]
1	None	-	-	-	-	-	0.01	0.64	32.76
2	4 element	Static	4.77	1.15	3.67	1.10	5.20	1.86	32.76
3	5 element	static	6.40	1.51	4.27	1.56	7.29	2.54	32.76
4	4 element	active	4.77	0.09	3.67	0.29	5.20	1.01	32.76
5	5 element	active	6.40	0.08	4.27	0.30	7.30	1.04	32.76

2.3.4 Lap Simulation Results

The baseline vehicle without aerodynamics has a simulated lap time of 56.53 seconds. Static aerodynamics packages of four and five-element wings reduce lap times by 1.06 and 1.31 seconds respectively. Note that the difference in lap time between both a four-element and five-element packages is only 0.25 second decrease in lap time. This is because although the car has a much higher lateral cornering capability, straight line speeds begin to suffer. The active wing packages in case four and five have the ability to manage drag on course. This results in greater straight line acceleration producing larger decreases in lap times. The four-element package results in a decrease in lap time by 1.92 seconds and the active five-element wing package reducing lap times by 2.83 seconds. The results are tabulated below in table 5. Screen captures of the simulations themselves can be found in the Appendix B.

Table 5. Lap Simulation Results.

Case	Wing	State	Lap time [s]	Dec. [s]
1	None	-	56.534	-
2	4 element	Static	55.470	-1.064
3	5 element	Static	55.225	-1.309
4	4 element	Active	54.611	-1.923
5	5 element	Active	53.704	-2.830

In autocross style racing, tracks are usually won or lost by fractions of a second. Based on the simulation times, the following conclusions can be drawn:

1. Even though the courses are designed for average speed of 35mph properly developed aerodynamics can reduce lap times significantly on the 2013 autocross course.

2. Being able to actively manage drag on course can result in a further reduction in lap time.

3. An active five element aerodynamics package will save the most time on track out of the five cases.

Based on the lap simulations, the active five element aerodynamics package will save 2.83 seconds per lap on the autocross course. This is a significant amount of time considering the margins for victory and top places are typically very small often differing by fractions of a second. The top ten places from autocross for the 2012 Lincoln competition are listed below along with the margin of victory.

Table 6. Margin of Victory for 2012 Lincoln Autocross [4].

Place	Lap Time [s]	Margin [s]
1	53.462	-
2	55.025	1.563
3	56.213	2.751
4	56.408	2.946
5	56.461	2.999
6	56.67	3.208
7	56.739	3.277
8	56.801	3.339
9	56.963	3.501
10	57.316	3.854

2.4 Top Speed

The Formula SAE rules dictate that courses designed for the competition should have average speeds of 35 mph and not exceed top speeds of 70 mph [5]. Also, based on the lap simulations, nearly 70% of the time spend on course is in some form of a turn.

This implies that cornering capability should be prioritized over top speed. Cars without aerodynamics are typically capable of well over 100 mph and are limited by gearing rather than drag. As a result, the top speed of these vehicles can be sacrificed for aerodynamic drag to improve the cornering capability.

The top speed for the 2013 car is first calculated in the non-active state. This is to ensure that car can still reach the expected top speeds and not be drag limited for high speed sweepers. Based on lap data taken from the 2012 competition autocross the top speed seen on course at the end of a straight was 53 mph [1].

Also currently under development is a new engine package for the 2013 car. The engine is based around the Yamaha YZF-450 engine used in the 2012 car. However, the engine will have significant internal modifications with a projected power output of 60 hp. This figure is used in all top speed calculations.

Calculating the top speed of the car is based on both the drag equation (2.1) and the power equation (2.1). Total drag on the vehicle is given by the equation below where ρ is the standard air density, V is the velocity of the vehicle, C_D is the total vehicle drag coefficient, and A is the frontal area of the vehicle.

$$D = \frac{1}{2}\rho V^2 C_D A \qquad\qquad 2.1$$

In addition, the propulsion force of the vehicle is given next where P is the power produced at the wheel, and V is vehicle velocity.

$$F = \frac{P}{V} \qquad\qquad 2.2$$

The top speed is defined when the propulsive force of the engine equals that of the drag force. Combining equations (2.1) and (2.2) above yields the final expression for top speed.

$$V = \left(\frac{2P}{\rho C_d A}\right)^{\frac{1}{3}} \qquad\qquad 2.3$$

Equation (2.3) is used to calculate the theoretical top speed of the 2013 FSAE car. Both the active and non-active states are shown in the next table as well as the top

speed of the car in its non-aero form for comparison. As shown, the car will still be able to reach the top speeds seen on track in the event the wings are used in a static manner.

Table 7. Theoretical top speed of the 2013 FSAE car.

State	C_d	A [ft^2]	Top Speed [mph]
No Aero	0.641	7.15	124
Active	1.04	10.2	94
Static	2.54	10.2	70

2.5 Acceleration Capability

Based on the lap simulations, an active five element wing package will be used on the F13 car. Another study is performed to calculate the acceleration capability through each gear both with static and active aerodynamics. To accomplish this engine data for the 2013 car is used along with gearing data to determine the acceleration potential of the vehicle. The aerodynamic drag force in both the static and active form is calculated to analyze the acceleration capability at any given speed.

2.5.1 Engine Dynamometer Data

Under development, for the 2013 race car is a new power plant projected to deliver 60 hp. As the engine package is still ongoing and being tested and tuned, actual dynamometer data is not available yet. However power curves for the engine in stock configuration are readily available. For the purpose of this simulation, the power curve will be projected by shifting it upwards to reach 60 hp. The projected dynamometer graph for the 2013 race car is shown below in figure 10. The relationship between torque and horsepower is also shown in equation (2.4). Note that the unit of power in equation (2.4) is in horsepower which results in units of ft-lbs for torque.

22
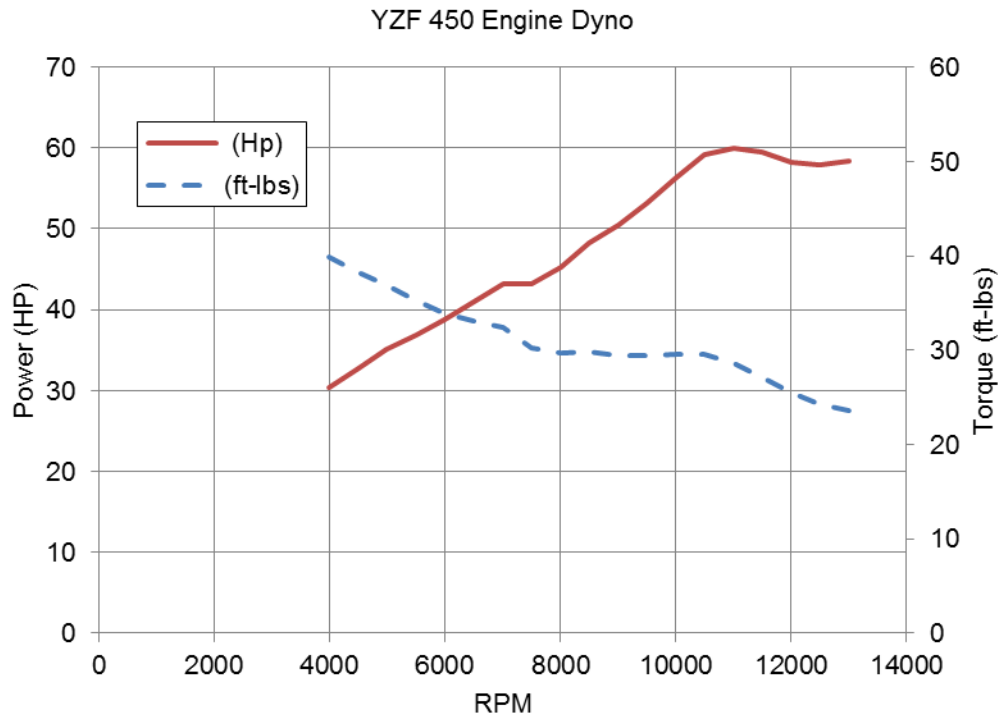
Figure 10. 2013 engine dynamometer data [1].

$$T = \frac{5252 * HP}{RPM}$$ 2.4

2.5.2 Propulsive Force at the Wheel

The propulsive force at the wheel is a product of the transmission ratios as well as the sprocket diameters and the diameter of the tire. The torque output of the engine is then multiplied by these ratios to calculate the propulsive force at the wheel. The equation for propulsive force at the wheel is given by equation (2.5).

Table 8. Drivetrain ratio for the 2013 car

Primary Reduction	2.652	:1
1st Gear	2.500	:1
2nd Gear	2.000	:1
3rd Gear	1.632	:1
4th Gear	1.300	:1
5th Gear	1.095	:1
Final Drive	3	:1
Tire Diameter	20.00	in

$$F_p = R_{pri} R_{gear} R_{final} d_{tire} T_{engine} \qquad 2.5$$

The propulsive force is normalized to the weight of the car to calculate the *g's* of propulsion. This normalized metric is a non-dimensional value referring to how hard the vehicle can accelerate. For example, accelerating at 1 *g* would be equivalent to 32.17 ft/s^2 or 9.81 m/s^2.

$$g_{prop} = \frac{F_p}{W} \qquad 2.6$$

The limit of the propulsion force in the lower gears is based on the traction limit of the tire. The actual limit can be calculated theoretically however track data has shown that under an acceleration launch, 1 *g* is typically the maximum acceleration force seen [1].

2.5.3 Aerodynamic Drag

The drag force of the five-element wings in both open and closed form is calculated using equation (2.1) above and is shown in the next figure. In additional to the aerodynamic drag, the rolling resistance or mechanical drag for the car is included in the total drag. It is measured to be around 2% of the weight of the car equaling 13.4 lbs of rolling resistance shown by the offset in the drag curves [12]. Equation (2.7) calculates rolling resistance of the vehicle. The total resistive force from both aerodynamic and mechanical drag is normalized to *g's* of deceleration.

24

$$F_{roll} = C_r W \qquad\qquad 2.7$$
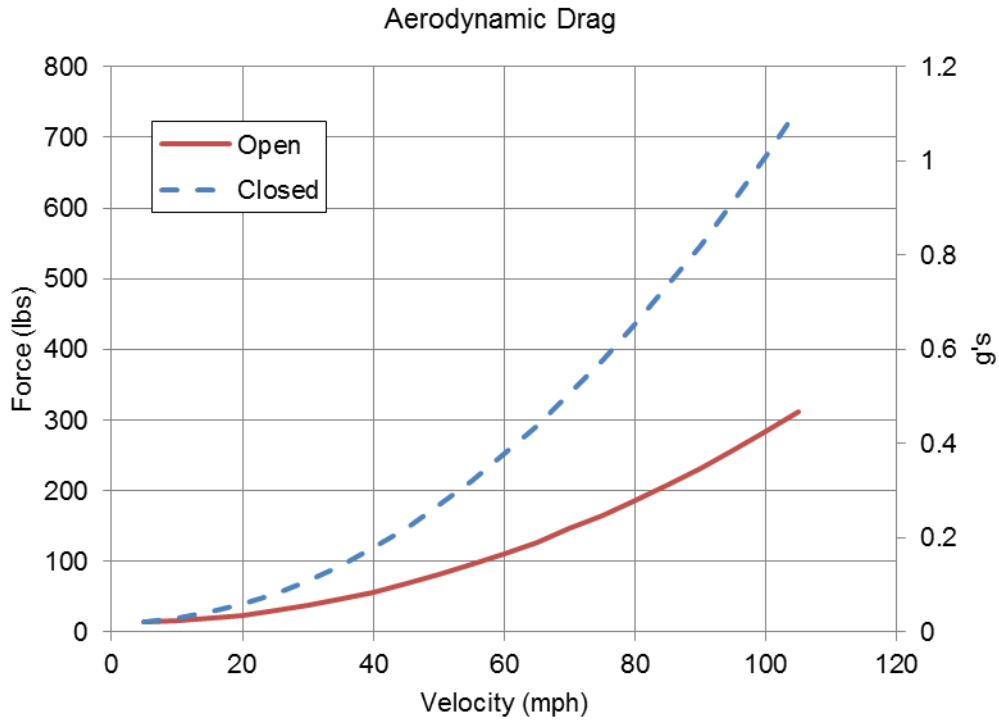
Figure 11. Aerodynamic drag force for 5 element wing.

2.5.4 Normalized Acceleration Capability

The ability of the vehicle to accelerate is governed by how many *g's* of force the tires can hold, as well as how many *g's* of drag force is being produced by the wings. At low speed, the tire limit of traction is assumed to be 1 *g*. At accelerations below the traction limit, the total acceleration is calculated with equation (2.8).

$$g_{accel} = g_{prop} - g_{drag} \qquad\qquad 2.8$$

Figure 12 shows the acceleration potential of the 2013 car calculated from the above equation and plotted versus speed. The gear ratios are shown as well indicating the maximum speed that can be reached in each gear. Note that the car is limited to 1 *g*

of acceleration in first gear. The solid lines indicate the cars acceleration ability with active aerodynamics and the dashed lines indicate static aerodynamics.

Acceleration Potential
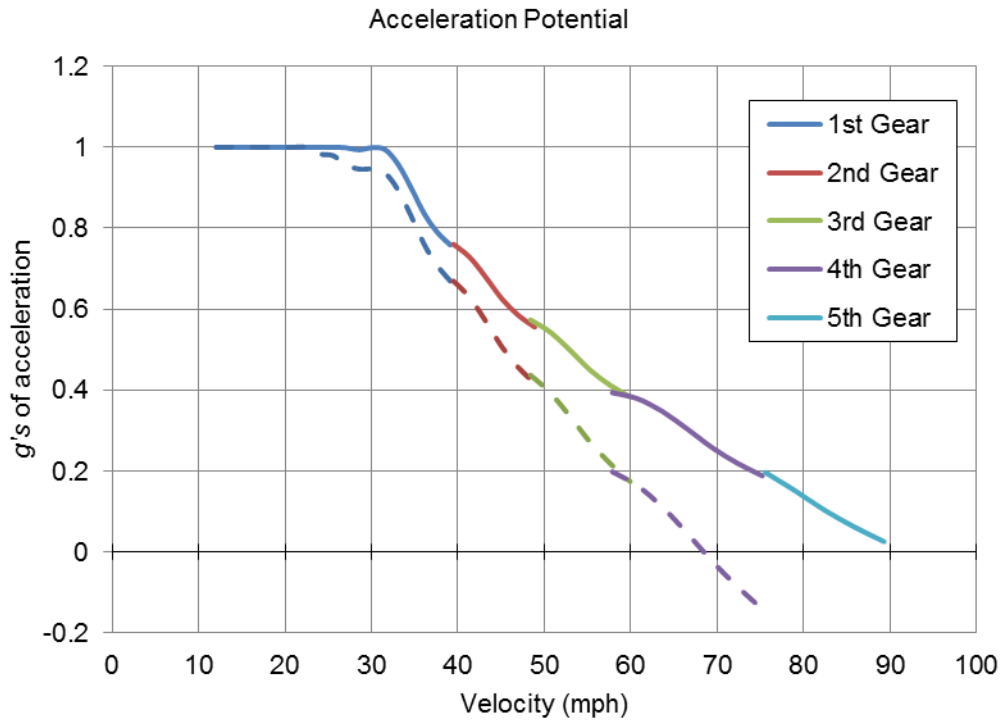
Figure 12. Acceleration capability of the 2013 car with active aerodynamics.

From figure 12, the difference between the solid and dashed lines indicates the amount of acceleration g's that can be obtained from opening the wings during straight line acceleration. Taking the difference of these two curves calculates the gains made. Since the typical driving range of an FSAE track is anywhere from 30 – 60 mph, this means that on a single straight the car can expect gains of 0.05 *g's* up to 0.2 *g's* of acceleration.

Chapter 3

Aerodynamic Design

3.1 Introduction

The aerodynamic design consists of 3D simulation of the rear wing. This data is used to calculating the forces and moments on each rotating flap. The moments are then used when designing the actuation system. Since the theoretical top speed of the race car with wings closed is 70 mph, the actuation system is designed to open the wings at 75 mph. This ensures that even at the drag limit, the actuators will not be overpowered by the loads on the wings and potentially damage system components.

3.2 3D Simulation Data for Five-Element Wing

The rear wing is further analyzed with a full 3D simulation results at 75 mph. This is slightly faster than the theoretical top speed of the vehicle calculated in Chapter 2 for the wings in the closed position. Data from this will be used to calculate the moments needed to articulate an individual flap.

3.2.1 Simulation Setup

The rear wing is first modeled in 3D using Solidworks. In order to save on computational time, only half the wing will be analyzed assuming that the flow is symmetric about the center-line. The wing is extruded at half span with an oversized endplate as shown in the next figure. Based on the simulation results, the large endplate will be reduced in size to minimize the tip vortices and spillage at the wing tips that ultimately increase drag and reduce the efficiency of the wing.
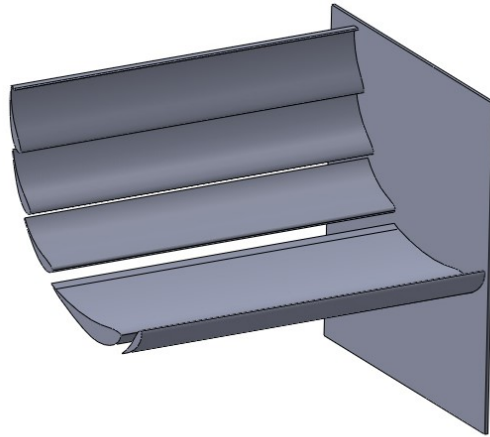
Figure 13. 3D Rear wing model.

The model is imported into Pointwise, stand-alone mesh generation software for grid generation and setting up the far-field boundaries. After grid generation, the mesh is importing into StarCCM+ for simulation. The wing is simulated using the K-epsilon turbulence model at 75 mph. Lift, drag, and moments are monitored on each element individually to ensure convergence. All moments are calculated about the leading edge of the main plane which is considered to be the origin of the wing. The simulation setup and procedure is the same in both the open and closed position.

3.2.2 Simulation Data

Simulation data for the wing in both the open and closed position at 75 mph is shown in table 9. The lift, drag, and moment produced by each individual wing element is given. All moments are references about the about the leading edge of the main plane. This data is used to calculate the pivot point location for the flaps as well as the torque required to rotate the element.

28

Table 9. Five-element aerodynamic data at 75 mph.

Part	Lift		Drag		Moment	
	SI	US	SI	US	SI	US
Endplate	-4.41 [N]	-0.99 [lbf]	-16.37 [N]	-3.68 [lbf]	-106.80 [N-m]	-24.01 [lbf-in]
Flap 1	-220.53 [N]	-49.58 [lbf]	-119.78 [N]	-26.93 [lbf]	-2773.28 [N-m]	-623.46 [lbf-in]
Flap 2	-81.43 [N]	-18.31 [lbf]	-120.15 [N]	-27.01 [lbf]	-1886.97 [N-m]	-424.21 [lbf-in]
Flap 3	-15.16 [N]	-3.41 [lbf]	-76.36 [N]	-17.17 [lbf]	-1037.08 [N-m]	-233.15 [lbf-in]
Mainplane	-591.27 [N]	-132.92 [lbf]	-9.88 [N]	-2.22 [lbf]	-2485.41 [N-m]	-558.74 [lbf-in]
Slat	-111.24 [N]	-25.01 [lbf]	89.70 [N]	20.17 [lbf]	235.90 [N-m]	53.03 [lbf-in]
Total:	-1024.03 [N]	-230.21 [lbf]	-252.84 [N]	-56.84 [lbf]	-8053.65 [N-m]	-1810.53 [lbf-in]

Part	Lift		Drag		Moment	
	SI	US	SI	US	SI	US
Endplate	-0.98 [N]	-0.22 [lbf]	-15.08 [N]	-3.39 [lbf]	-93.16 [N-m]	-20.94 [lbf-in]
Flap 1	-40.65 [N]	-9.14 [lbf]	-7.50 [N]	-1.69 [lbf]	-517.74 [N-m]	-116.39 [lbf-in]
Flap 2	-27.76 [N]	-6.24 [lbf]	-6.28 [N]	-1.41 [lbf]	-462.19 [N-m]	-103.90 [lbf-in]
Flap 3	-32.89 [N]	-7.40 [lbf]	-8.27 [N]	-1.86 [lbf]	-616.47 [N-m]	-138.59 [lbf-in]
Mainplane	-188.20 [N]	-42.31 [lbf]	0.01 [N]	0.00 [lbf]	-783.39 [N-m]	-176.11 [lbf-in]
Slat	15.30 [N]	3.44 [lbf]	-13.03 [N]	-2.93 [lbf]	-61.55 [N-m]	-13.84 [lbf-in]
Total:	-275.19 [N]	-61.87 [lbf]	-50.16 [N]	-11.28 [lbf]	-2534.51 [N-m]	-569.78 [lbf-in]

3.3 Pivot Point Calculations

The pivot point calculations for the flaps will determine how much torque is required to actuate the flap. This is accomplished using the line of pressure rather than the center of pressure of each element. This concept is useful when the center of pressure does not necessarily lie on the body itself or has excessive movement. This is especially true of cambered wings. The line of pressure is defined simply by the resultant of lift and drag into the net aerodynamic force acting on a single element. Its position is given by dividing the moment produced by the flap about an axis, which in this case is the leading edge of the main plane, and dividing by the resultant force will give the perpendicular distance from that point. This is shown in figure 14.
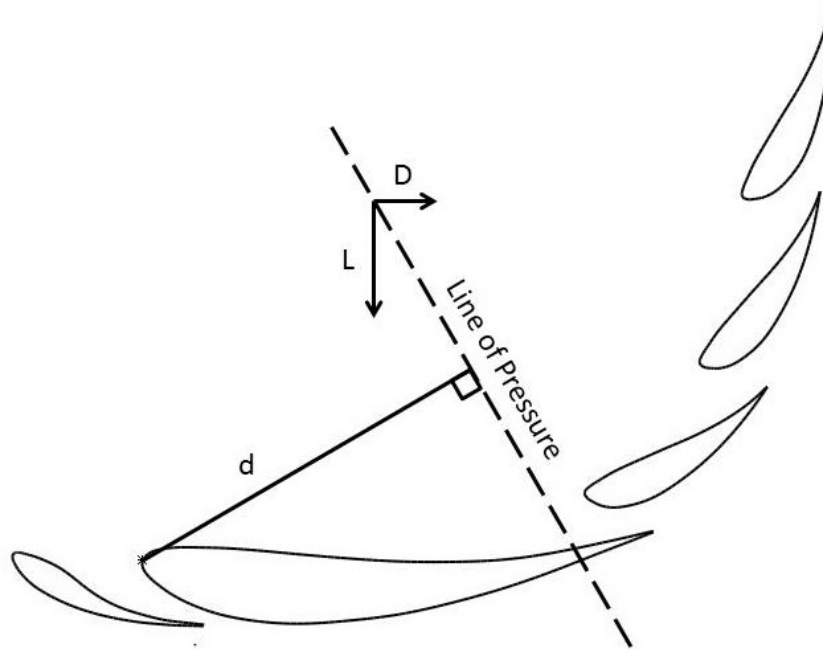
Figure 14. Line of pressure on a multi-element.

The following design constraints are used when determining the position of the pivot location relative to the flap.

1. The pivot location will be the same for each flap element on both the front and rear wing.

2. The point will be positioned such that the wing will aerodynamically stay either open or closed depending on its orientation.

3. The pivot location will be designed such that the torque required to open and close the wing will be the same.

The first design criteria are important due to the manufacturing of the car. Time constraints are very tight and any time commonality between parts can be established, it will save time during production.

The second design criterion is established to improve the efficiency of active aerodynamic system. Depending on the actuation method, the wings will be able to hold their position aerodynamically with mechanical stops rather than constantly consuming energy to hold the wing in its state. This is especially important when using an electronic actuation system. In this case, the actuators will be powered off the vehicle battery and depending on current draw and power output of the engine, can deplete the battery over the endurance race. With this design criterion, when the wings are in the closed position, they will remain as such without consuming any power. Likewise when the wing begins to open, the elements will reach an aerodynamic tip over point where they will start opening by themselves and stay open. Depending on the sophistication of the electronics and programming, various power saving techniques could be employed such as turning off the servos unless a disturbance or change in angle of attack Is required.

The last criterion is to ensure that the actuation system can be sized as small as possible to reduce the weight penalty and improve its energy efficiency.

For a cambered at high angle of attack, wing the center of pressure is near the aerodynamic center or the quarter chord point. As the wing begins to open, the center of

pressure migrates aft of the wing and the aerodynamic force produced by the wing is greatly reduced. Placing the pivot location just aft of the center of pressure in the closed position will most likely achieve these criterions. Figure 15 and Figure 16 demonstrates the line of pressure migration of flap undergoing a change in angle of attack.
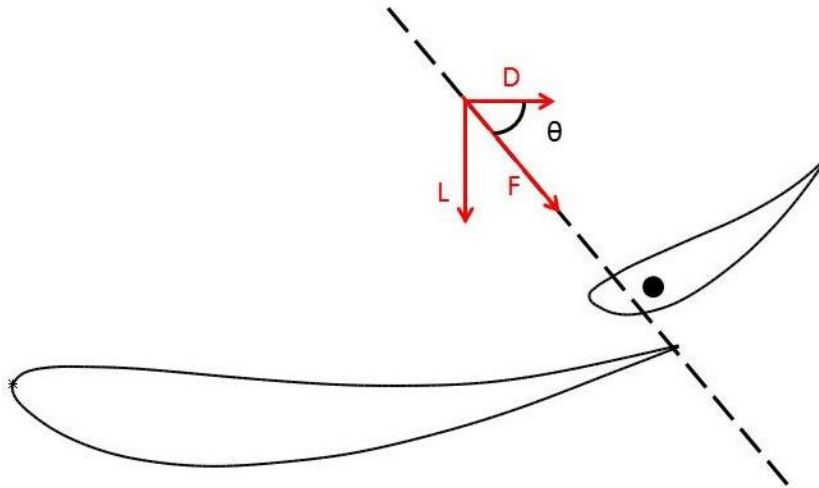

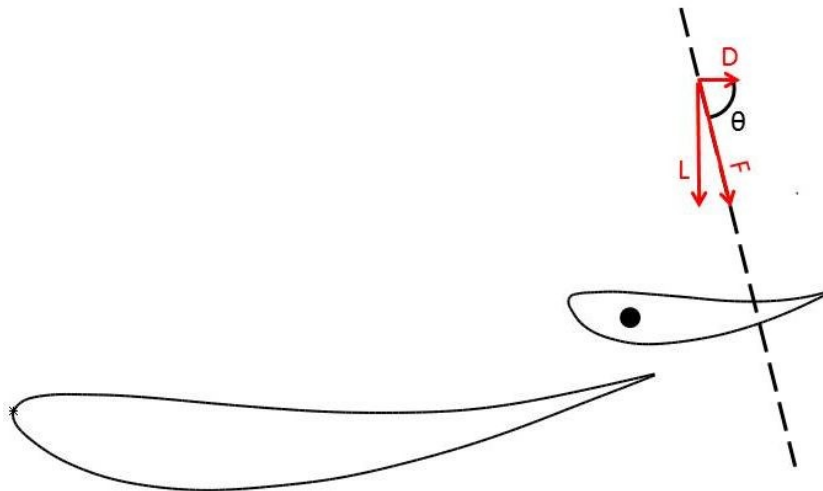Figure 15. Line of pressure migration on a closed element.

Figure 16. Line of pressure migration on an open element.

The wing pivot locations are calculated based on equation (3.1) below with x_p and y_p being the coordinates of the pivot location with respect to the leading edge of the flap, x_b and y_b is the flap position with respect to main plane, θ is the angle of the line of pressure (Appendix C), α is the angle of attack of the individual flap, F is the resultant aerodynamic force, and M_w is the moment about the leading edge of the main plane. The derivation of this equation can be found in Appendix C.

$$M_{Pivot} = F\left(x_p \cos(\theta - \alpha) + y_p \sin(\theta - \alpha) + x_B \cos\theta + y_B \sin\theta - \frac{M_W}{F}\right) \qquad 3.1$$

The moment arm from the line of pressure and the resultant moment about the flaps for the rear wing is given in table 10.

Table 10. Pivot point moments on the flaps for a half rear wing.

	d_{close}		M_{close}		d_{open}		M_{open}	
Flap 1	0.28	[in]	15.95	[lb-in]	1.75	[in]	-14.94	[lb-in]
Flap 2	0.18	[in]	5.96	[lb-in]	1.03	[in]	-6.44	[lb-in]
Flap 3	0.07	[in]	1.21	[lb-in]	0.66	[in]	-5.29	[lb-in]

The moment calculations show that the first flap has the largest moment produced in the closed position. On the rear wing, the first flap produces 24% of the total load produced by the wing. The second and third flaps together produce 14% and 7% of the total resultant load produced by the wing respectively.

The pivot locations satisfy all design criteria listed above. First, each flap is successfully designed with the same pivot location thus reducing the number of parts to be manufactured. Also based on the line of pressure migration, the moment produced by the flap elements allow for the wing to stay in its position aerodynamically. Finally, for each element, the torque required to both open and close the wings is designed to be of

equal magnitude. This ensures that the required torque to actuate the wings is at its minimum value. The third flap was not able to completely satisfy the third design criteria however since it carries the smallest load from the wing; the difference in torques is small.

The same procedure is performed with the front wing. The same pivot location used for the rear satisfies the same design criteria for the front wing. This ensures part commonality amongst all elements.

Chapter 4

Philosophy, Initial Design, and Control Schemes

4.1 Introduction

Active aerodynamics is set apart from a basic DRS in its ability to be autonomous and transparent to the driver as well as its ability to optimize the wing configuration for any given track scenario. In order to take full advantage of an active aerodynamics system, the appropriate control method and schemes must be developed. The inputs required by the driver to active the system is important to take into consideration and will have the biggest effect on the functionality of the system. Several types of actuation systems can be used such as pneumatic, electrical, or electro-mechanical.

4.2 Control Philosophies

In autocross style racing each course is different and racers will never see the same course twice. Course layouts vary greatly in design ranging from more open courses consisting of long straights and large sweepers to more technical low speed courses. Autocrossers are not able to practice the tracks and thus rely on their ability to read tracks and understand and drive at the performance limits of the car. The addition of a drag reduction system to an FSAE car adds a new dimension to the performance envelope of the car allowing for higher straight line accelerations which also allows for higher corner entry speeds and reducing lap times.

4.2.1 Types of Control

There are three main types of control that can be used for a drag reduction system of which various implementations can be used. Each type of control requires varying levels of input from the driver. The three categories of control schemes are driver activated, driver initiated, and full active control.

4.2.1.1 Driver Activated Control

Driver activated is the simplest as far as functionality and allows for two wing states, fully-open and fully-closed. This method of control is accomplished by the driver on track and usually involves pushing and holding a button on the steering wheel to open the wings. Releasing the button closes the wings. This system requires the driver to be in the decision loop constantly thus increasing their work load. Activation is typically limited to the longest straights where the driver has time to gauge the point at which to open the wings. The consequence of opening or closing the wings too soon or too late in a corner will result in a loss of traction. Figure 17 shows the driver input required for this control scheme.
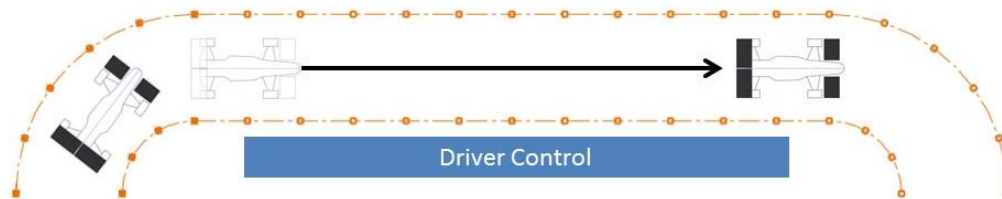
Figure 17. Driver actuated control on a straight.

4.2.1.2 Driver Initiated Control

Driver initiated control is the next step in sophistication with regard to activating drag reduction. The driver is still limited to the two wing states of open and closed as in the previous control scheme; however triggering the wings to open or close only requires one input from the driver. Upon exiting a corner and entering a straight away, the driver activates the drag reduction by some method such as a button on the steering wheel and the wings stay in their open position until another input is given from the driver to close the wings. This can be accomplished either by pressing a button again or more

commonly triggering, the wings to close when applying pressure to the brakes. This control scheme is shown in figure 18.
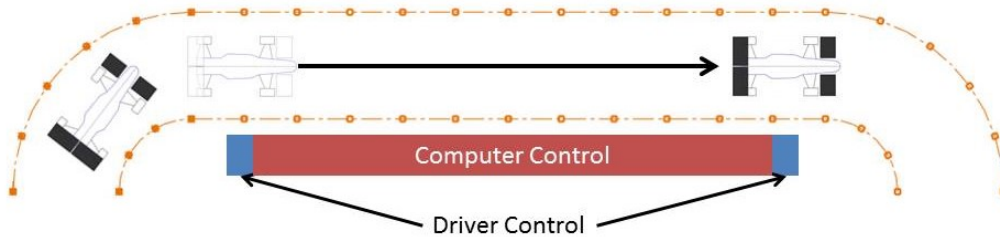
Figure 18. Driver initiated control on a straight.

4.2.1.3 Active Control

Active control of a drag reduction system allows for the system to be completely autonomous to the driver as activation is accomplished by a computer system taking sensory input of different vehicle parameters and calculating when to open and close the wings. Also since the system is electronic based and depending on the type of actuator used the wings are no longer limited to just two states but can have multiple states not just in flap position but also allow for different quadrants of the wings to be in different states at the same time. Depending on the sophistication of the electronics, active control can actuate the wings sooner than both driver activated and driver initiated control and also with more precision. This control scheme is shown in figure 19.

Figure 19. Active control on a straight.

4.2.2 Wing Actuation

Many different methods exist for actuating the flaps on a multi element wing. Each method has different applications and advantages dis-advantages. The most common methods currently found in Formula SAE include pneumatic, direct electronic, and electro-mechanical.

4.2.2.1 Pneumatic Actuation

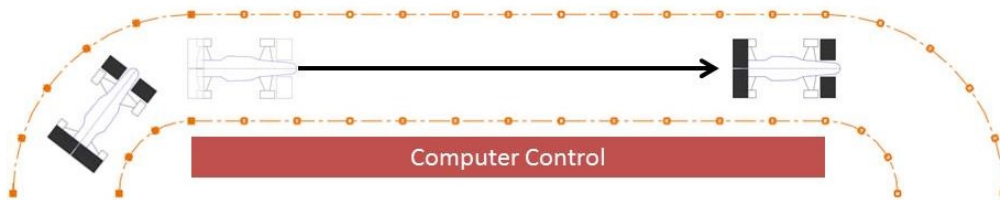Pneumatic systems have the advantage of being simple and reliable. Actuators are powered by a high pressure tank which is regulated down to an operating pressure that produces the actuation force. For a drag reduction application, a double acting cylinder will be required to both open and close the wing. This type of cylinder is shown in figure 20.

Figure 20. Double acting pneumatic actuator.

Pneumatic actuation has been the most popular method to implement a drag reduction system in Formula SAE. The disadvantage to this type of actuation only allows for the wings to only two states, open and closed. Also in the case of a multi-element wing design, multiple actuators need to be used or a robust mechanical linkage used to connect the flaps together which can result in a heavier system.

Based on the aerodynamic loads calculated in Chapter 3 and assuming all the wing elements are linked, the cylinder and linkage need to produce a total of 26.7 in-lbs of moment per half wing. Assuming an one inch moment arm the actuator requires a

minimum of 27 lbs of force to move the wing from a closed position. This is calculated for half of a wing. The required pneumatic cylinder was sourced and weighs approximately 0.7 lbs for one cylinder. Actuating both the front and rear wing will require four double acting cylinders for a preliminary system weight of 2.8 lbs not including the weight of the air tank or linkage.

Missouri S&T is one team that utilizes a pneumatic actuation system. Their 2013 car utilizes a single rear actuator with a mechanical linkage connecting two rear flaps together. An example of their pneumatic style actuation system is shown in figure 21.

Figure 21. Missouri S&T Pneumatic DRS.

4.2.2.2 Direct Electronic Actuation

Electronic actuation systems consist of using servo motors to directly actuate the elements. Servos have advantages of being very compact and powerful; especially those used for large scale hobby RC applications. These servos come in various torque outputs and speeds. Servos are controlled via pulse width modulation (PWM) which allows for very controlled, fast, and precise movement. An example of a large scale RC servo motor is shown in figure 22.

Figure 22. Large Scale RC Servo.

Direct electrical actuation involves mounting servos in the wing elements themselves. Controlling all elements of a five-element wing would require a minimum of twelve servo motors. However a major disadvantage to this system is the packaging of the servo in the wing element. The flaps require the wing profile to be modified in order to fit accommodate the size of the servo. Assuming the same servo is used for all wing elements and sized appropriately to actuate the largest flap load of 15 in-lb, the required servo will weigh approximately 0.165 lb. Using twelve servos to actuate both the front and rear wing totals a preliminary system weight of 1.98 lbs not including the weight of the electronic components to generate the pulse width signal.

Oklahoma Formula SAE team utilizes a direct electronic actuation system. The modification to the rear wing elements removes approximately three inches out of the effective wing span. A close up of the servo bumps in the rear wing can be seen in figure 23.

Figure 23. University of Oklahoma wing with servos embedded into wing elements.

4.2.2.3 Electro-Mechanical Actuation

Electro-mechanical actuation is similar to direct electronic actuation. It too used servo motors to move the wings however it is coupled together with a linkage system so that elements can be actuated together. This is advantageous in a multi element wing system because it can limit the number of physical actuators needed to move all the wing elements. This also allows for the servos to be packaged in the main plane thus maintaining the wings aerodynamics. Based on the pivot point calculations performed in Chapter 3, the moments produced by the second and third flap together are equivalent to that of the first flap. Linking these flaps together, will reduce the number of servos required to eight thus reducing the approximate system weight to 1.32 lbs

4.3 Initial Design

The aerodynamics system for the 2013 car will utilize active control of the wings via an electro-mechanical actuation system. In order to maximize the gains of a full aerodynamics package the wings should be controlled autonomously and without driver input. This eliminates whatever driver training would be required to actuate the wings based on the track and allows the driver to focus on the course.

The active aerodynamic system will be developed as a for not just drag reduction but also as a platform for even more advanced control schemes such as aerodynamic anti-dive and anti-roll which can aid the driver on track and further reduce lap times. To allow for development, the system is designed for individual control over each quadrant of the car. The four wing quadrants are shown in figure 24.
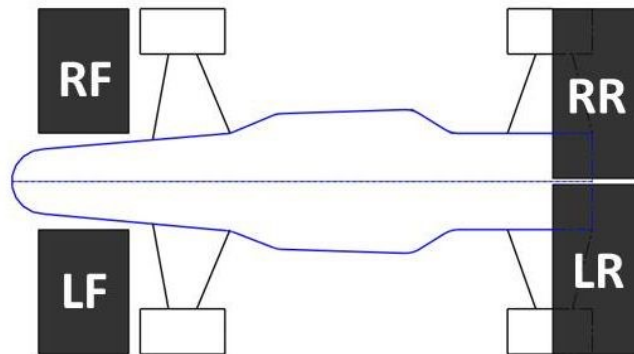

Figure 24. Wing quadrants on the 2013 FSAE car.

4.3.1 Component sizing

The calculated moments on each flap element based on the pivot point calculated in Chapter 3 are shown in table 11. The first flap requires the highest torque to rotate at 16 in-lbs to move from the closed position while the second and third flaps require a much lower torque.

Table 11. Flap moments from chapter 3.

	M_{close}		M_{open}	
Flap 1	15.95	[lb-in]	-14.94	[lb-in]
Flap 2	5.96	[lb-in]	-6.44	[lb-in]
Flap 3	1.21	[lb-in]	-5.29	[lb-in]

In order to reduce system weight, both the second and third flaps can be linked together via a mechanical linkage and be operated off a second servo. The torque required for each servo in this scenario is shown in table 12.

Table 12. Total torque required by servos.

Servo	Flap	Topen		Tclose	
1	1	15.95	[lb-in]	-14.94	[lb-in]
2	2&3	7.17	[lb-in]	-11.73	[lb-in]

The servo selected for actuation produces a total torque of torque of 26.9 lbf-in with a no-load speed of .118 sec/60°. This selection was made to ensure that the wings can actuate quickly and also allow for the linkage to be designed appropriately.

4.3.2 Component layout

Each wing quadrant uses two servo motors to actuate the wing flaps. These servo motors will mount inside the main plane with an access panel built into the upper surface of the wing for access. A mechanical linkage connects the servos to the individual wing elements. The servo labeling convention as well as the fitment into the main plane is shown in figure 25.
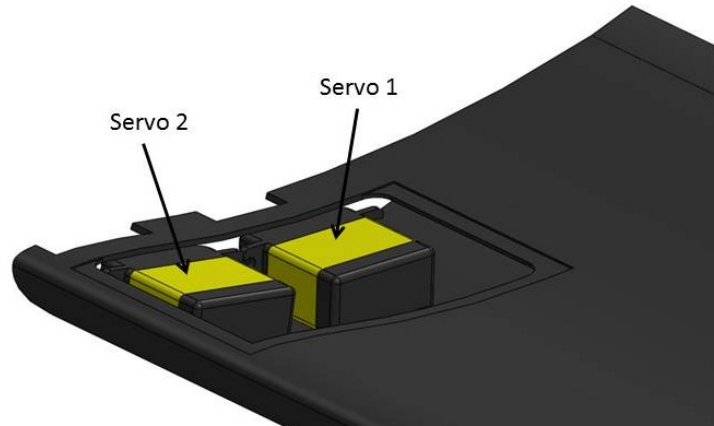
Figure 25. Servo motors packaged in the main plane.

4.3.3 Active Aero Computer

All eight servos are controlled by a microcontroller located at the center of the car. The controller receives input from the vehicle sensors and then generates the PWM signal to actuate each wing quadrant. The primary parameter used for controlling the wings is lateral and longitudinal *g's*. The controller board itself has a stand-alone accelerometer as well as the ability to read other sensors on the car over a controller area network (CAN) bus. A global view of the car with all eight servo locations as well as the computer is given in figure 26.
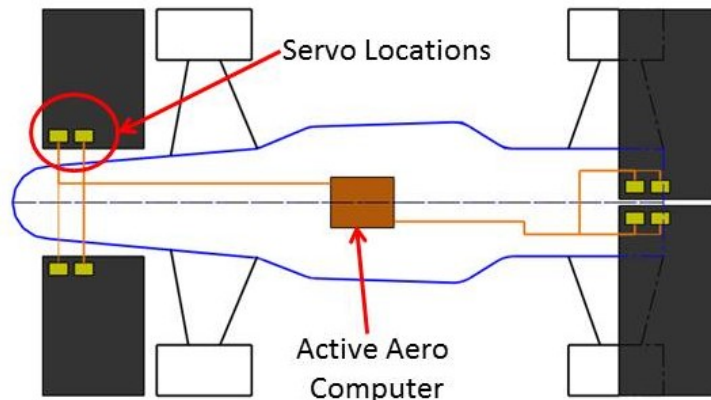

Figure 26. Component layout.

4.4 Control Schemes

A total of three different controls schemes will be used with the active aero system. Each scheme then has two separate modes that it can operate under. There are four different dynamic events at the competition; skid pad, acceleration, autocross and endurance that each have specific requirements for the wings. The control schemes incorporated into the active aerodynamic system include active control, fixed state control, and diagnostic controls.

4.4.1 Active Control

Active control is the primary mode used on the active aerodynamic system. Each wing quadrant can be individually controlled and managed based on data from the onboard accelerometer. Two different aerodynamic profiles can be programmed to aid the tuning process by directly comparing different settings on track.

4.4.2 Fixed-State Control

Fixed-state control is used to maintain the wings in either an open or closed position. These modes are important for the acceleration event where a minimum drag configuration needs to be maintained at all times and the skid pad event where a maximum downforce configuration is needed.

4.4.3 Diagnostic Control

Two different diagnostic functions are given to analyze the wings. First a DRS mode limits the wings only open and closed states. This is a driver actuated control scheme which allows for direct comparison of lap times between fully active control and driver activated mentioned previously. The second diagnostic mode is used to test the servo motors themselves. A pre-programed pattern of different movement combinations will display the servos moving through its range of motion collectively and individually to diagnose the system in the event of a servo problem.

Chapter 5

Flap Actuation Linkage

5.1 Introduction

The actuation system consists of servo motors mounted in the main plane

coupled with a light weight linkage that connects to the three flaps of the five-element

wing. The first servo motor controls the first flap which has the highest load on it. The

second motor is linked to the second and third flap.

5.2 Linkage Design

Two design considerations are taken into account when analyzing the control

linkage. The flaps need to articulate through their full range of motion from initial angle of

attack to their minimum drag position at zero angle of attack. This prioritizes the motion

ratio of the linkage which will dictate the lever arm lengths. Also, the input arms for the

servos are limited to what is commercially available. Each servo has a spline drive

requiring a specific arm known as a servo horn. These arm lengths can be sourced in

0.25" increments.

5.2.1 Linkage Analysis

The linkage connecting the flaps together consist of three four-bar linkages

derived using an analytical synthesis method which can be found in Robert Norton's book

Design of Machinery [13]. The linkage is analyzed using a vector loop calculation. This is

taken by treating each link as a position vector and summing all the links together then

setting the equation equal to zero [13]. The vector loop equation is given by equation

(5.1). The derivation of this equation and its use in analyzing the linkage kinematics are

given in Appendix D.

$$\boldsymbol{R2 + R3 - R4 - R1 = 0} \qquad\qquad 5.1$$

5.2.2 Linkage Design

The equations discussed in Appendix D are programmed into Matlab to analyze the motion ratio of the linkage as well as the mechanical advantage and velocity ratios. Both link c and link d are fixed based on the element placement as well as maintaining proper clearance through the range of motion of the flap. Links a and b were iterated to get the correct motion ratio. A linkage depicting all the relevant links is shown in figure 29.
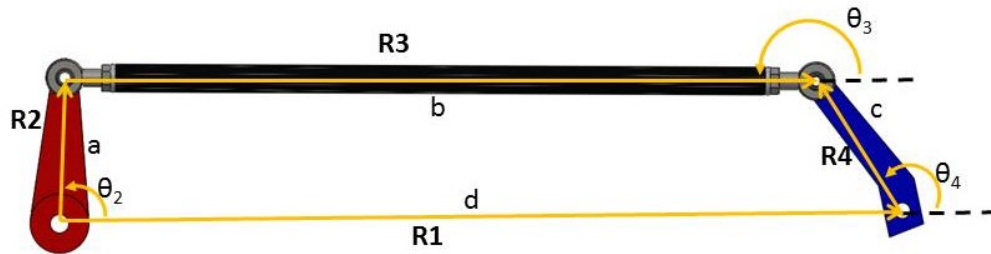

Figure 27. Flap linkage with appropriate nomenclature.

The linkage for the second servo, this consists of two four-bar linkages. The first linkage connects the servo motor with the second flap while the second linkage connects the second and third flaps together. The linkage in its open and closed position can be seen in figure 28 and figure 29.
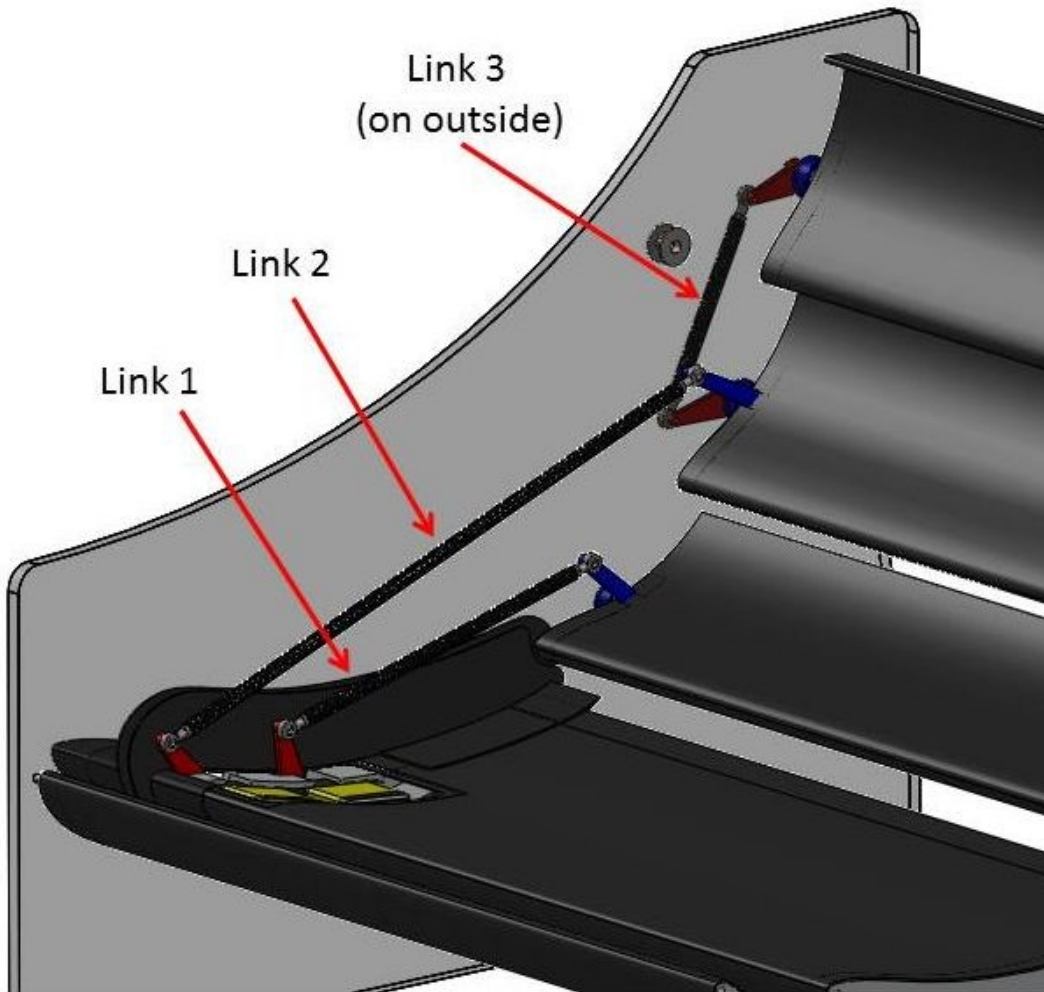
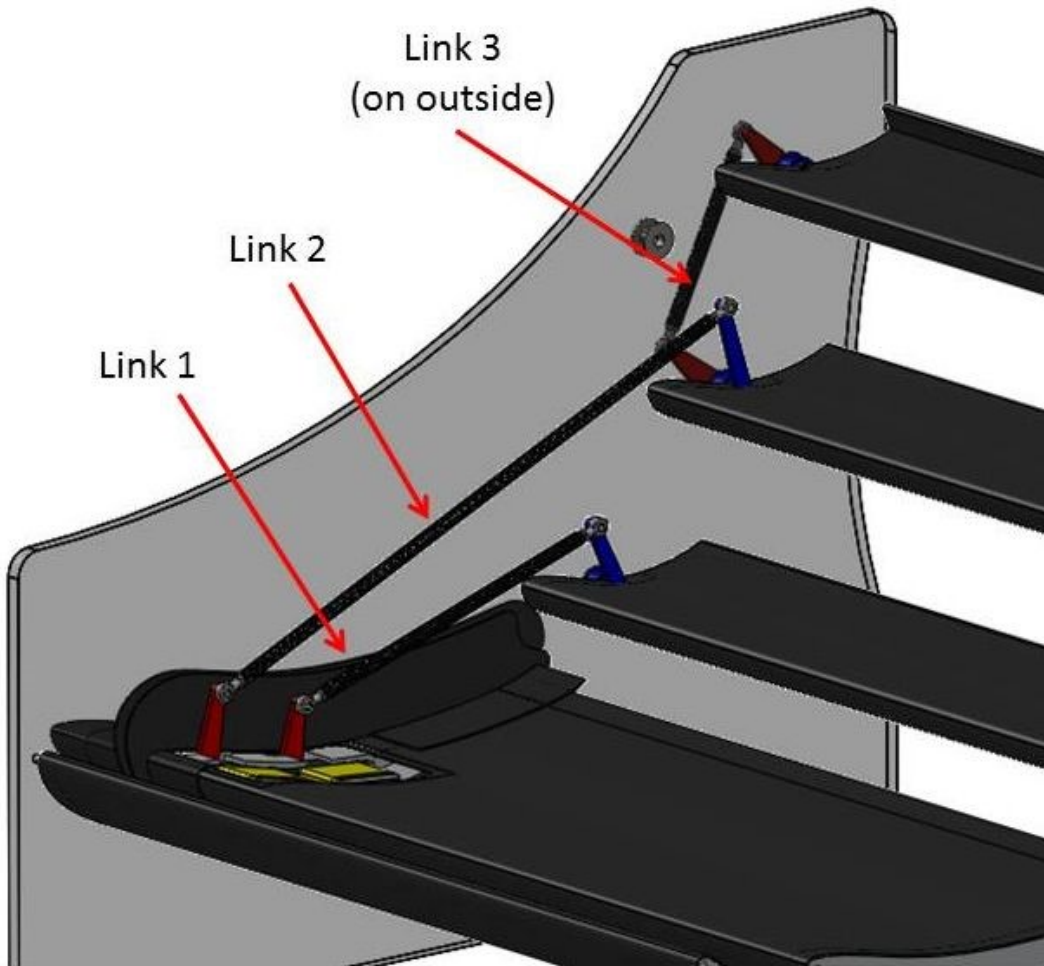Figure 28. Linkage connecting individual flaps together in the closed position.

Figure 29. Linkage connecting individual flaps together in the open position.

5.3.3 Servo Loads through the linkage

Since the linkage for each flap is not a one to one ratio, the loads at the servo are be verified to check that each servo can still articulate the wing elements. This is done using the same method described in Appendix D. The mechanical advantage of each linkage is calculated at the open and closed position of the linkage and then multiplied by the aerodynamic moment produced by the flaps. This calculated the final torque required at the servo which is still below the limits of the servo. Appendix E shows the kinematics of each linkage as a function of the normalized angle of attack of flaps or percentage open.

Chapter 6

Electronic Design and Tuning

6.1 Introduction

The design and implementation of the embedded electronics system was done in conjunction with electrical engineering student Randy Long. His responsibilities include the design of the active aero control board itself, its fabrication as well as the programming and debugging of the electronics as well as implementing the different control schemes to for the wings. The tuning of the wings is accomplished by individual lookup tables for each quadrant of the car.

6.2 Electronic Design

The active aero controller is mounted at the center of the car. Three separate wiring harnesses then branch out to connect to each wing as well as the dash of the car so the driver can change between different wing modes. Figure 30 below shows the active aero control board.
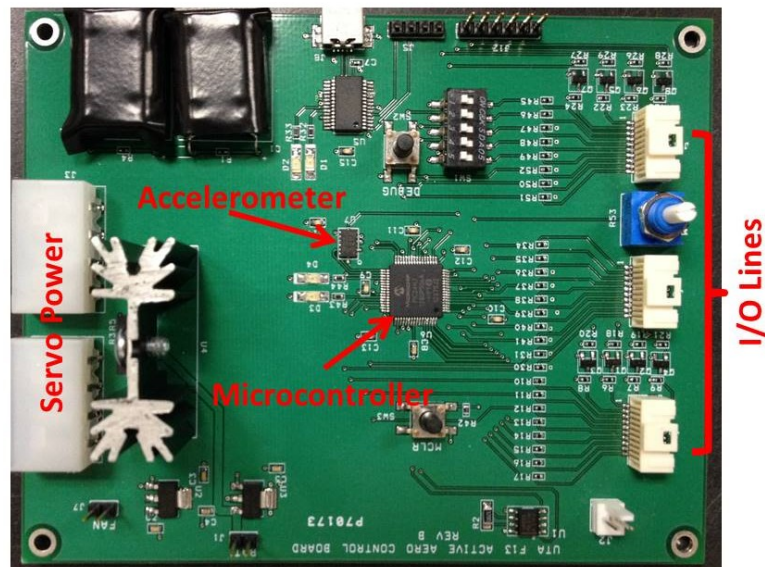

Figure 30. Active Aero Control Board.

The driver has the capability in the cockpit to change the control scheme of the car via a rotary switch on the dash and also to change the control mode by holding a button on the steering wheel when powering on the system. This is shown in figure 31.
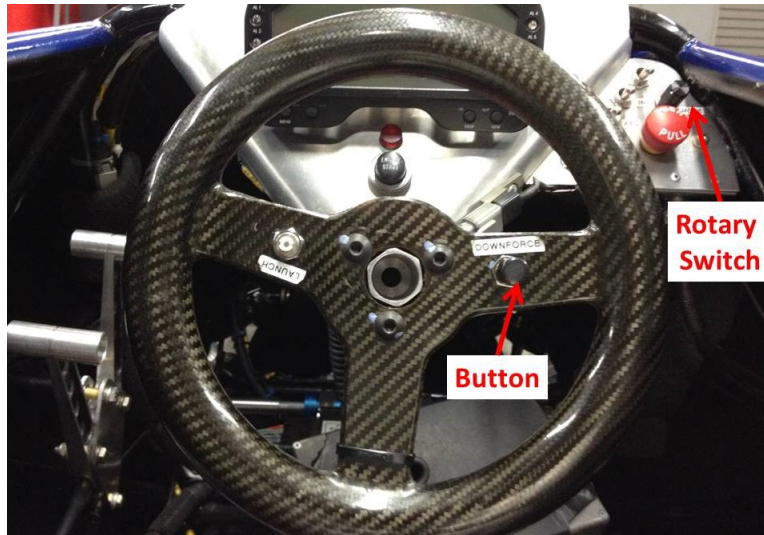

Figure 31. Driver inputs.

6.3 Active Mode Tuning

The active control scheme for the F13 car requires the wings to be tuned both for the car and driver ability. Two different active aero map settings are programmed to aid the tuning process. Each quadrant is controlled via a polar plot style look up table that dictates the wing position based on a given *g's*. The polar plot for the time history of the *g's* is referred to as the *g-g* diagram.

6.3.1 Sample Look-Up Table

A sample look-up table for one quarter wing is shown in figure 32. The table is created in excel using a *g-g* diagram reference indicated by the blue circles. A value from 0% to 100% is entered in each part of the table indicating wing state at the specific location in the table. The table has a resolution of 0.1 *g* per division and is tunable up to 2 *g's*. After this threshold the wings default to a closed state. The lookup table shown in

figure 32 would be used for a two state active DRS system. The solid green indicates the wings in an open state with the table values being 0%. Solid red indicates a 100% closed state. For a simplified active DRS, this map would be the same for each wing quadrant.
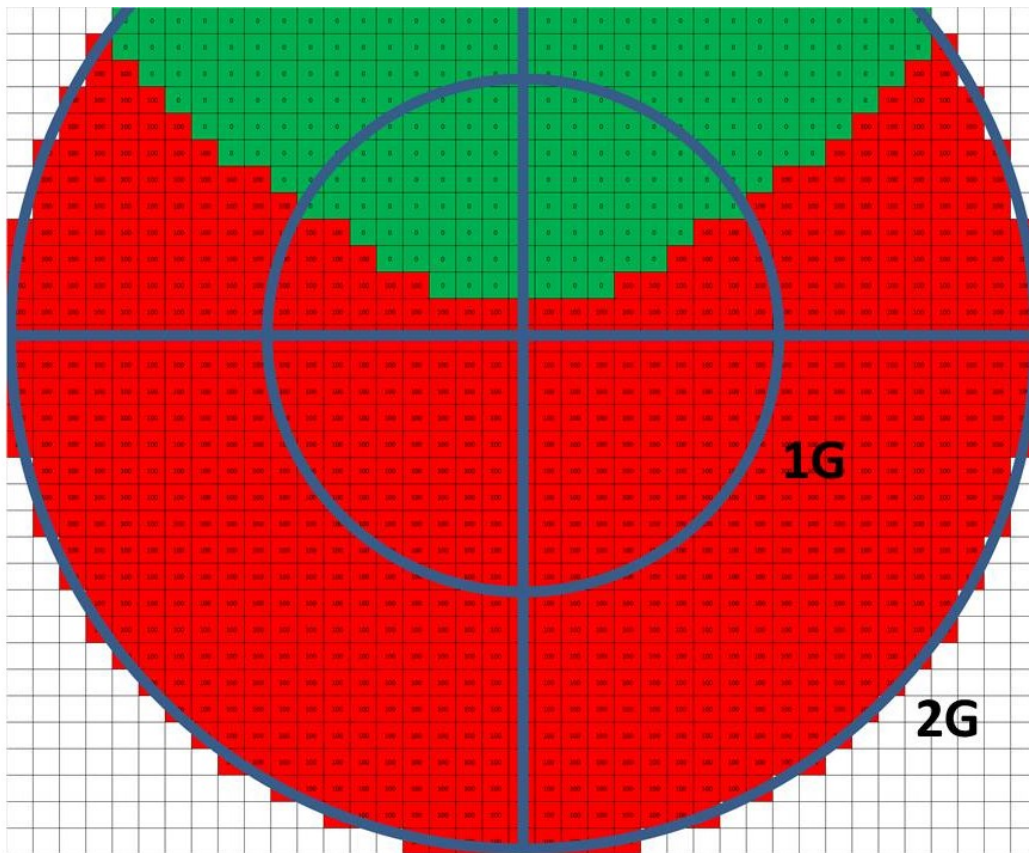

Figure 32. Aero map for one quarter wing with 2 state active DRS.

Chapter 7

Aeroelasticity and System Dynamic Response

7.1 Introduction

A complete math model of the active aerodynamics control system is developed to analyze the time response for the system to reach steady state assuming a change in from angle of attack from fully-open to fully-closed. This transition happens upon corner entry after straight line acceleration. This maneuver is shown below in the next figure. The transition time indicated below is the total time for the system to respond to the change in acceleration when the driver starts decelerationg. This time is based on the sum of individual transients of the electronics, actuation system, and the aerodynamic response of the wings. This is expressed in equation (7.1).

$$t_{trans} = t_E + t_C + t_A$$ 7.1
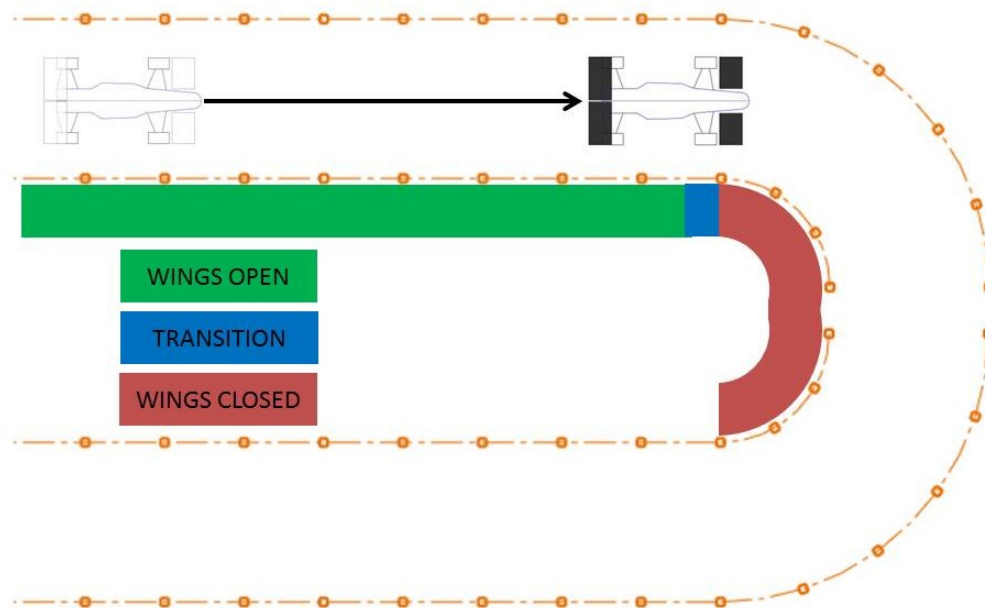

Figure 33. Transition from fully open to fully closed on corner entry.

7.2 Control System Modeling

Each component of the wings is modeled individually and then linked in Matlab for simulation. figure 34 gives the flow diagram for the simulation as well as each model used and its corresponding outputs. A total of four different models are used; this includes steady state aerodynamics, linkage kinematics, servo output, and an unsteady aerodynamics model. Each of these models discussed in more detail in reference [11].
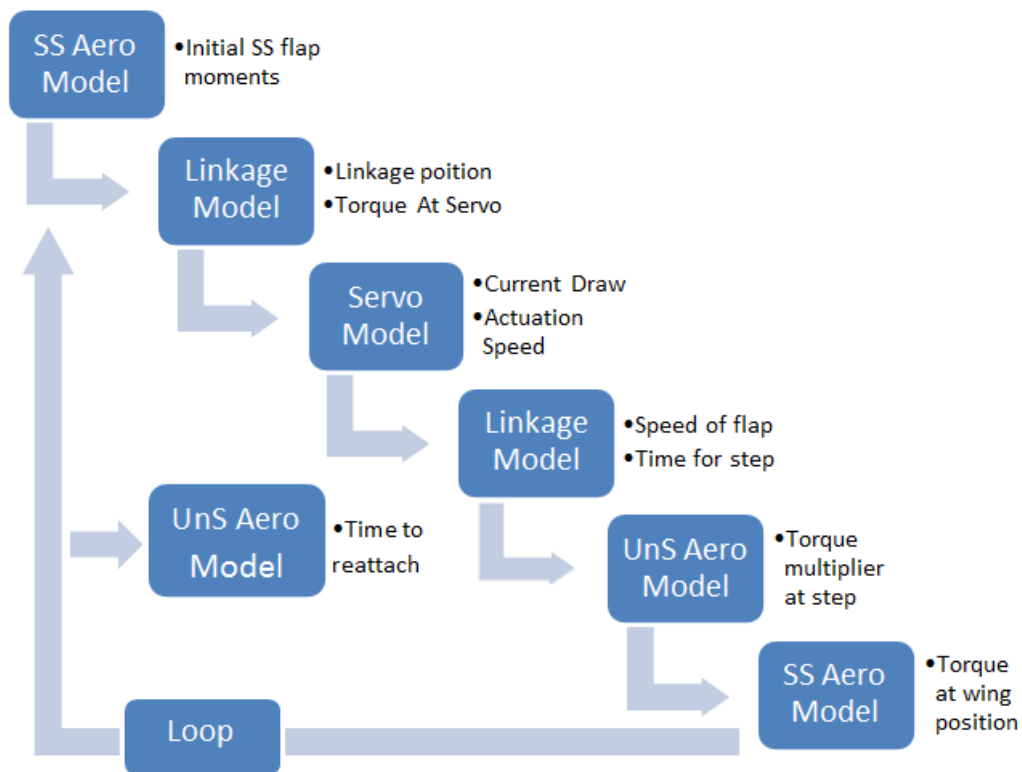

Figure 34. Model for time to reattach.

7.2.1 Steady State Aerodynamics Model

This model is based on CFD data generated in 2D. Equation (7.2) calculates the aerodynamic moment produced on each flap based on its normalized position.

$$M = \frac{1}{2}\rho v^2 Sc \left(\frac{dC_m}{d\alpha}\alpha + C_m\right)$$

<div align="right">7.2</div>

The moments produced on each flap versus normalized angle of attack are shown in figure 35. When the moment on each flap reaches zero, this indicates the line of pressure is moving through the pivot location.
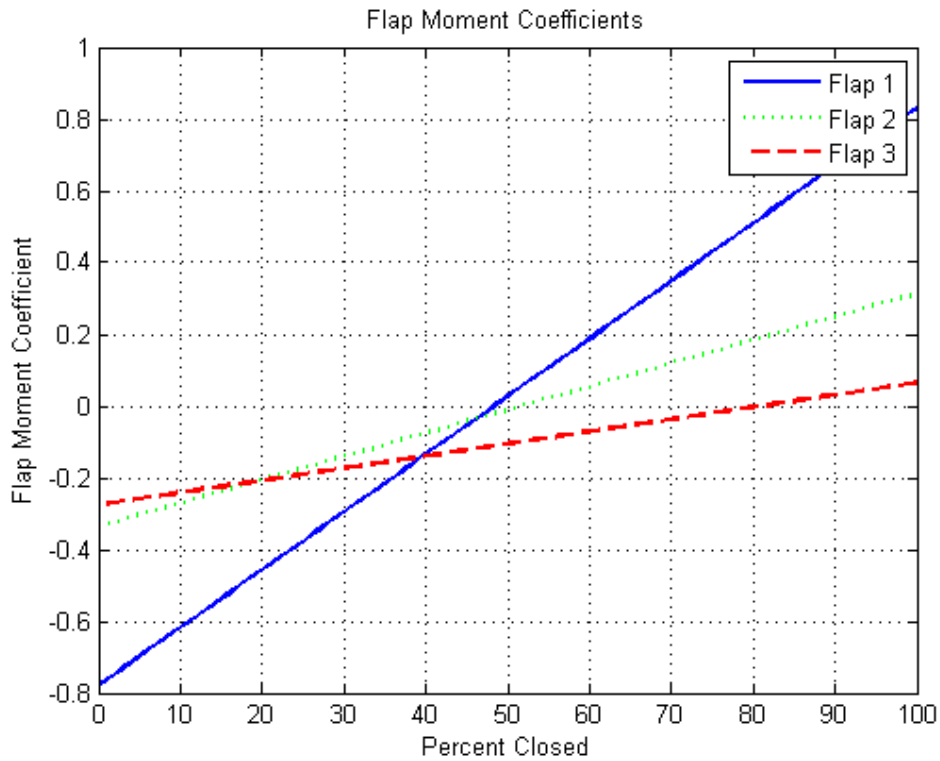

Figure 35. Flap moment coefficient vs percent closed.

7.2.2 Servo Motor Model

The model for the servo motors is derived based on manufacturer data and an idealized servo motor. The models for servo speed and servo torque are given by equations (7.3) and (7.4) below. The assumption of an idealized servo motor implies that the servo constants K_v and K_t are equal [15].

$$\omega = K_v T + \omega_{no\ load} \qquad\qquad 7.3$$

$$T = K_t I \qquad\qquad 7.4$$

Both torque and speed are inverses of each other. A servo operating at its no low speed which is specified by the manufacturer is working without any torque load on it. Rather, a servo workiLinkang at its maximum holding torque is assumed to have a speed of zero. The characteristics of the servo in the active aero system are shown in figure 36.
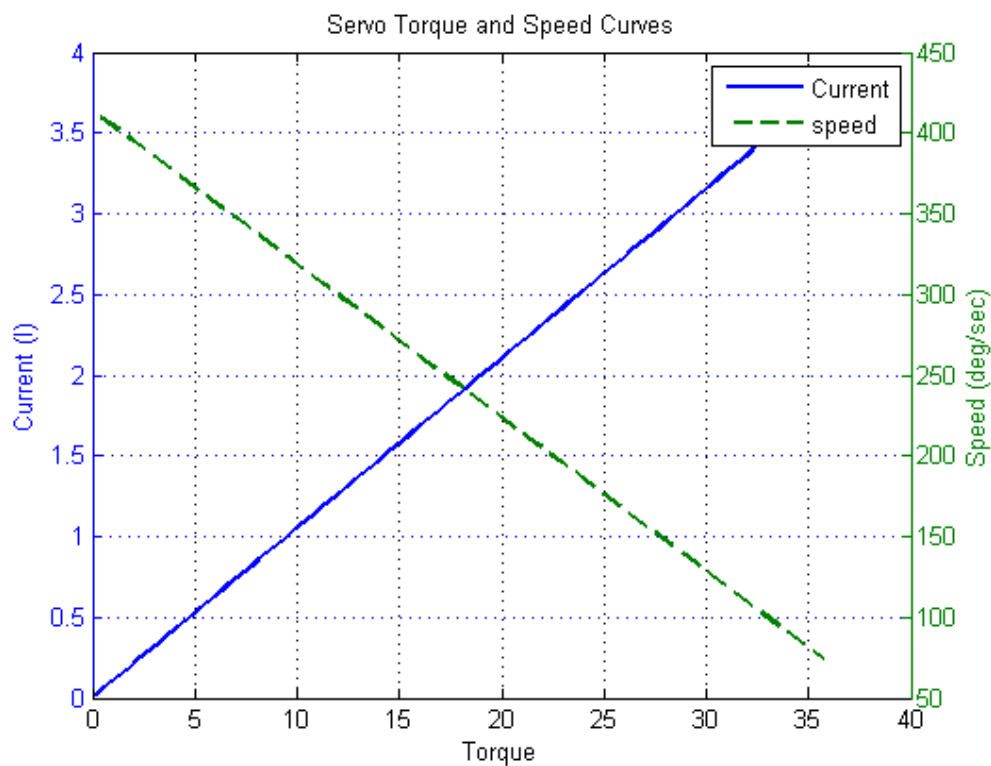

Figure 36. Servo torque and speed model.

7.2.3 Control Linkage Kinematics

The kinematic model of the linkage is based on the vector loop method discussed in Chapter 5. Based on this model, the motion ratios, mechanical advantage ratio and velocity ratios are calculated throughout the range of motion of each linkage.

These ratios are multipliers that affect the transmission of forces from the wing element to the servo. The characteristics of the linkage controlling the flaps are given in Appendix E.

7.2.4 Unsteady Aerodynamics Model

The unsteady aerodynamics model is based on the aeroelastic analysis the flaps individually. The problem itself is incredibly complex but is simplified to get an approximate value using the following assumptions.

1. The flow is attached throughout the range of motion of the flaps

2. The change in angle of attack can be modeled by a series of impulse changes in angle of attack

3. The flap elements themselves are assumed to be flat plates.

Based on these assumptions, Wagner's function can be used to approximate the time needed to reattach the flow of the wings. Wagner's function theorizes that for an impulse change in angle of attack, an airfoil will develop 50% of its maximum lifting value before settling to its maximum lift state. The full Wagner function is given by the sum of several Bessel functions as shown in equation (7.5) [6].

$$\varphi(\tau) = 1 - \int_0^\infty \{(K_0 - K_1)^2 + \pi^2(I_0 + I_1)^2\}^{-1} e^{-x\tau} x^{-2} dx \qquad 7.5$$

Several simplified approximations have been given for Wagner's function and have shown to be within 2% of the full function experimentally. The expression used for modeling unsteady aerodynamics is given in equation (7.6) where ε_1 and ε_2 are constants experimentally derived for a flat plate.

$$\varphi(t) = 1 - \varphi_1 e^{-\varepsilon_1 Ut/b} - \varphi_2 e^{-\varepsilon_2 Ut/b} \qquad 7.6$$

At t = 0, Wagner's function gives a value of 0.5 indicating that 50% of steady state lift will be produced and governs the time required to fully attack the flow based on the free stream velocity.

7.3 Model Results

All of the models are combined together to calculate the time needed to actuate the wing from fully open to fully closed. This is calculated both in the time domain given in seconds on the bottom of figure 37. The time is also normalized to transit periods of the wing or how many chord lengths the wing must travel to fully attach the flow given by the top scale. The model, the servos are able to actuate the wings to close in about 130 milliseconds. After this, it takes 70 milliseconds to reach 90% of the maximum lift coefficient produced by the wing. This equates to 2.4 transit times to reestablish the flow.
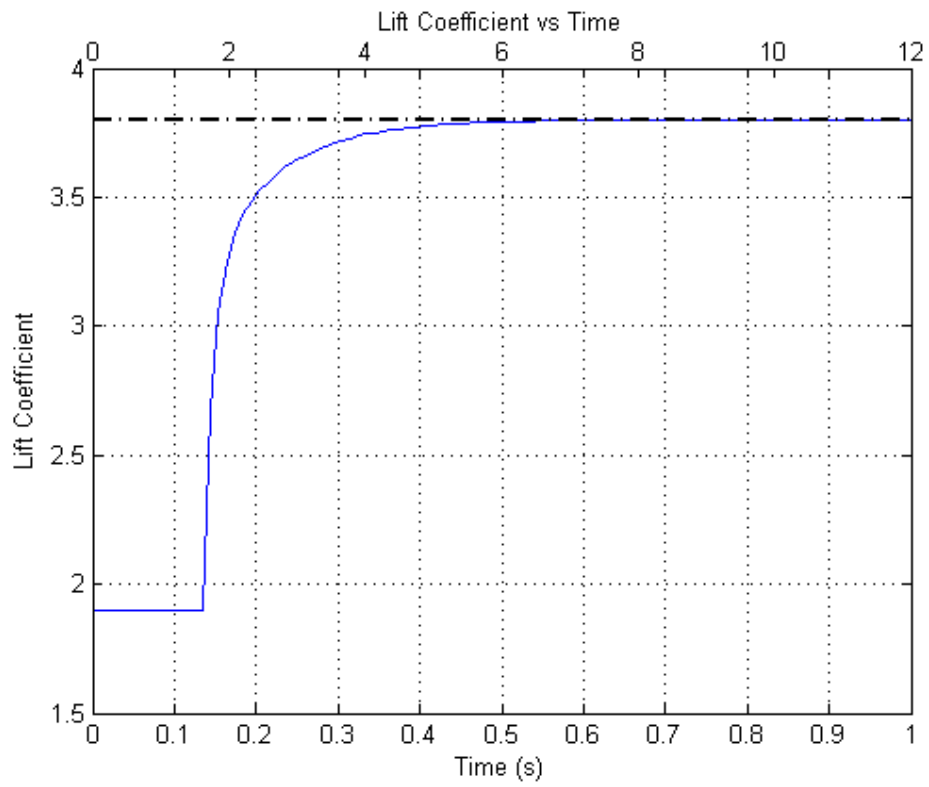
Figure 37. Time to reattach at 60 mph.

Chapter 8

Build and Implimentation

The active aerodynamics system is built and installed on the 2013 FSAE car. All components that are used in a quadrant are shown below in figure 38. The weight of the entire active aerodynamic system totals 3.66 lbs. A complete parts list as well as the individual weights of each component is given in Appendix F.
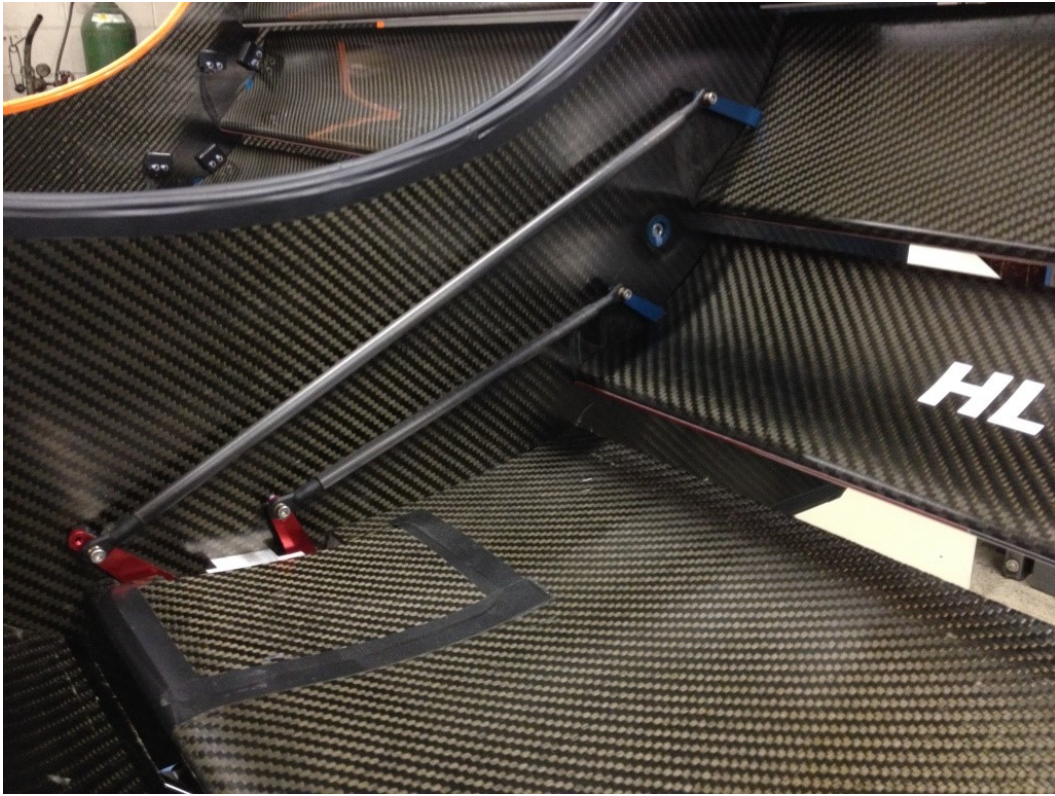

Figure 38. Components for rear quarter wing.
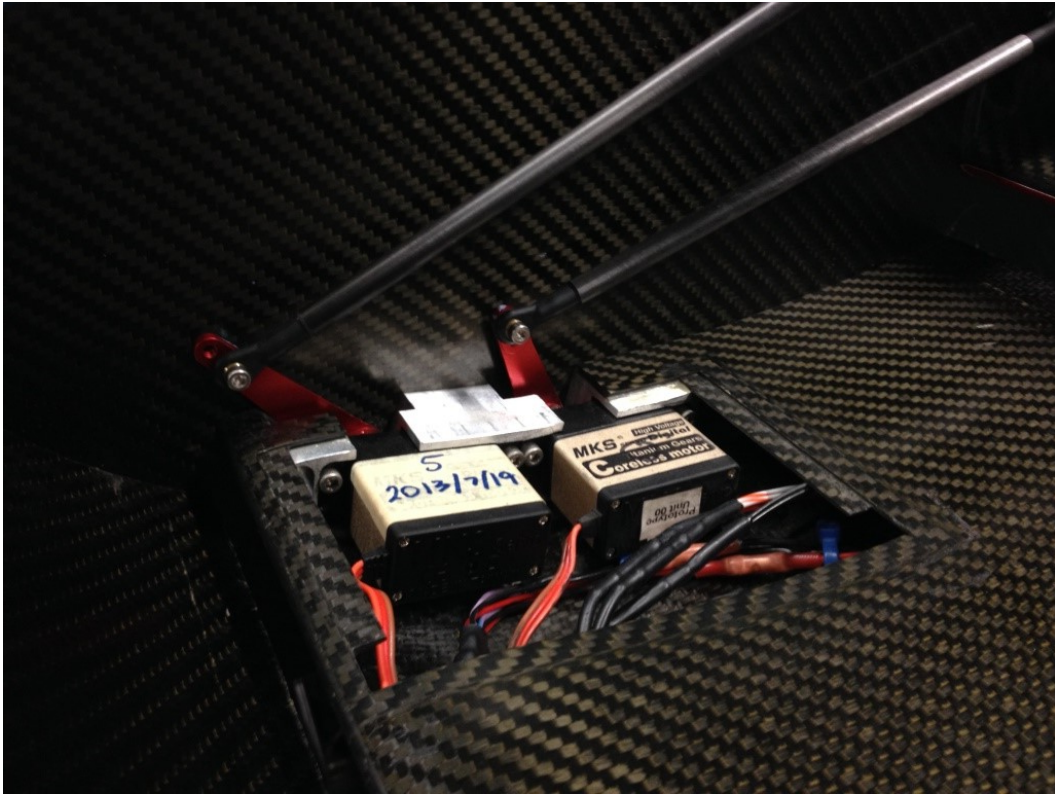
Figure 39. Rear wing in the closed state.

Figure 40. Actuation servos and linkage.

Figure 41. 2013 Formula SAE car with active aerodynamics.

Chapter 9

Conclusions and Future Work

9.1 Conclusions

The 2013 Formula SAE car is designed to incorporate an active five element wing that autonomously actuated on track to configure the car optimally for any given scenario. The wing profile itself is extensively studied to calculate an appropriate pivot location for the flaps to rotate around. This location is selected to minimize the moments required to open and close the flaps as well as use the line of pressure migration to maintain the flap in its open or closed position. The elements themselves are actuated using a servo motor coupled with a mechanical linkage connecting the elements together. The servo motors are housed in the main plane to preserve the aerodynamics of the wing. The servos are actuated via an on board computer that has three different control schemes to tune the car for the different dynamic events at the FSAE competition. The active aerodynamic system was successfully developed and implemented on the 2013 Formula SAE car. Preliminary testing has verified the functionality of the system and its viability on track.

9.2 Future Work

The active aerodynamic system is meant to serve as a platform for future development. Currently track testing utilizing aerodynamic anti dive under heavy braking has shown promise in improving the stability of the car. Other stability management control schemes can be experimented with as well such as aerodynamic anti roll.

Currently the tuning of the aero maps is the most cumbersome portion of operating the active aerodynamics system. Measures are being taken in a second generation approach to speed up this process by incorporating the system tuning onto an SD card rather than had coded onto the microcontroller.

Another aspect currently being addressed is noise on the pulse width lines due to operating the servos at higher voltages. This is also addressed in the second generation system by implementing a CAN network with nodes that generate the pulse width signal at the servo rather than sending the signals through several feet of wire when generated at the center of the car.

Appendix A

Corrections for 3D Effects on a 2D Wing Profile

Lift and drag coefficients are calculated from the data in Table 1. The lift and drag values are simulated at 30 mph and standard atmosphere conditions. The equations for 2D lift coefficient (A.1) and 2D drag coefficient (A.2) are shown below with lowercase subscripts *l* and *d* signifying two dimensional coefficients and *c* being the chord length of the wing.

$$C_l = \frac{2l}{\rho v^2 c} \qquad\qquad\qquad A.1$$

$$C_{d_0} = \frac{2d}{\rho v^2 c} \qquad\qquad\qquad A.2$$

To correct for 3D effects, both the actual aspect ratio and effective aspect ratio which include the effect of endplates is needed. The endplates greatly reduce the tip losses of the wing by separating the upper and lower wing surfaces. This results in an increase in wing efficiency by reducing the induced drag created at high lift conditions. The endplates were approximated according to the vertical height of the wing as shown in figure 42.
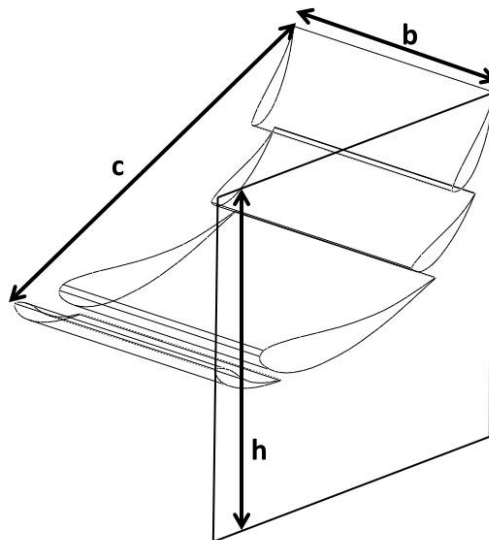

Figure 42. Approximate endplate sizing for both 4 and 5 element wings.

The aspect ratio for a wing is given by the equation (A.3) where b is the span of the wing and c is the chord.

$$AR_{actual} = \frac{b}{c}$$

A.3

The effective wing aspect ratio which corrects for the effect of endplates is found in *Race Car Aerodynamics* [7]. Equation (A.4) is shown below where h is the total height of the endplate shown in figure 42 and b is the wing span.

$$AR_{eff} = AR_{actual}\left(1 + 1.9\frac{h}{b}\right)$$

A.4

The effective aspect ratio is used to then calculate the induced drag. This is given in the next equation where C_l is the 2D lift coefficient, AR is the effective aspect ratio calculated in equation (A.5), and e is the efficiency factor of the lift distribution. For an elliptical lift distribution the factor is set to 1.

$$C_{d_i} = \frac{C_l^2}{\pi e AR_{eff}}$$

A.5

Equation (A.6) and (A.7) calculate the 3D lift and drag coefficient for the wing profile. The approximate lift coefficient is simply given by the 2D lift coefficient and drag is the sum of both viscous and induced drag. The 3D coefficients are denoted with capital L and D subscripts. These values are calculated for both the four and five-element wings and used in the lap simulation tool.

$$C_L = C_l$$

A.6

$$C_D = C_{d_o} + C_{d_i}$$

A.7

The front wing will contain the same element profiles for the main, slat, and flap but go through its own optimization in ground effect. The aspect ratio will be smaller because the mid-section of the wing is removed to fit around the nose of the car. Also the endplate sizes are different because of its close proximity to the ground. The same

procedure is used to calculate 3D effects as shown above section with the addition of a

correction factor for ground effect. *Competition Car Aerodynamics* shows the potential

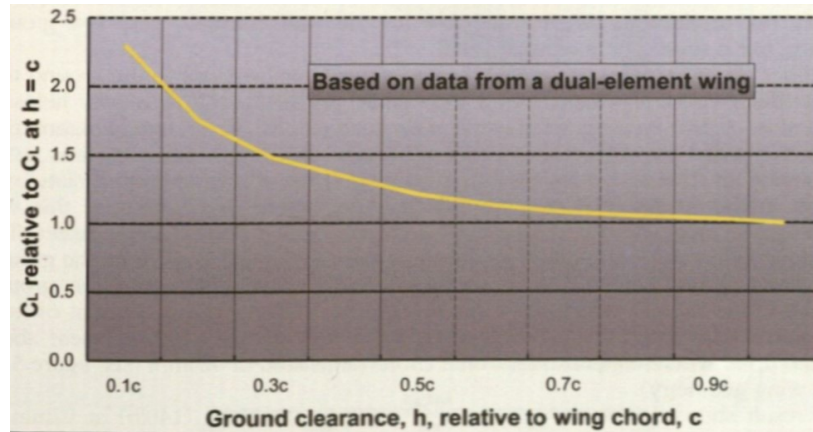gains that can be made from ground effect.

Figure 43. Influence of ground effect on wing performance [7].

The front wing of the car will operate in the area of 4 – 5 inches off the ground.

This corresponds to a ground effect factor of approximately 1.3 for the four-element wing

and 1.5 for the five-element wing. The final lift and drag coefficients for the front wing are

corrected using these factors as shown in the next two equations (A.8) and (A.9) where *G*

is the ground effect factor.

$$C_L = GC_l \qquad\qquad \text{A.8}$$

$$C_D = \frac{\left(C_{d_o} + C_{d_i}\right)}{G} \qquad\qquad \text{A.9}$$

Appendix B

Lap Simulation Results

Vehicle

Cd =	0.641	
Cl =	-0.007	Xcp
(based on frontal		-1896

Diffuser

Cd =	0.09	Xcp	60.00
Cl =	0.635	Xrd (in)	15.33
(based on plan		Zrd (in)	1.75

Front Wing

Cd =	1.10	Xcp	10.56
Cl =	4.51	Xrwf	28.91
(based on plan		Zrwf	4.75

Rear Wing

Cd =	0.92	Xcp	9.20
Cl =	4.33	Xrwr	63.00
(based on plan		Zrwr	31.00

Total

Total Cd =
Total Cl =
(based on frontal

Xcp Aero (from the front

Calculate
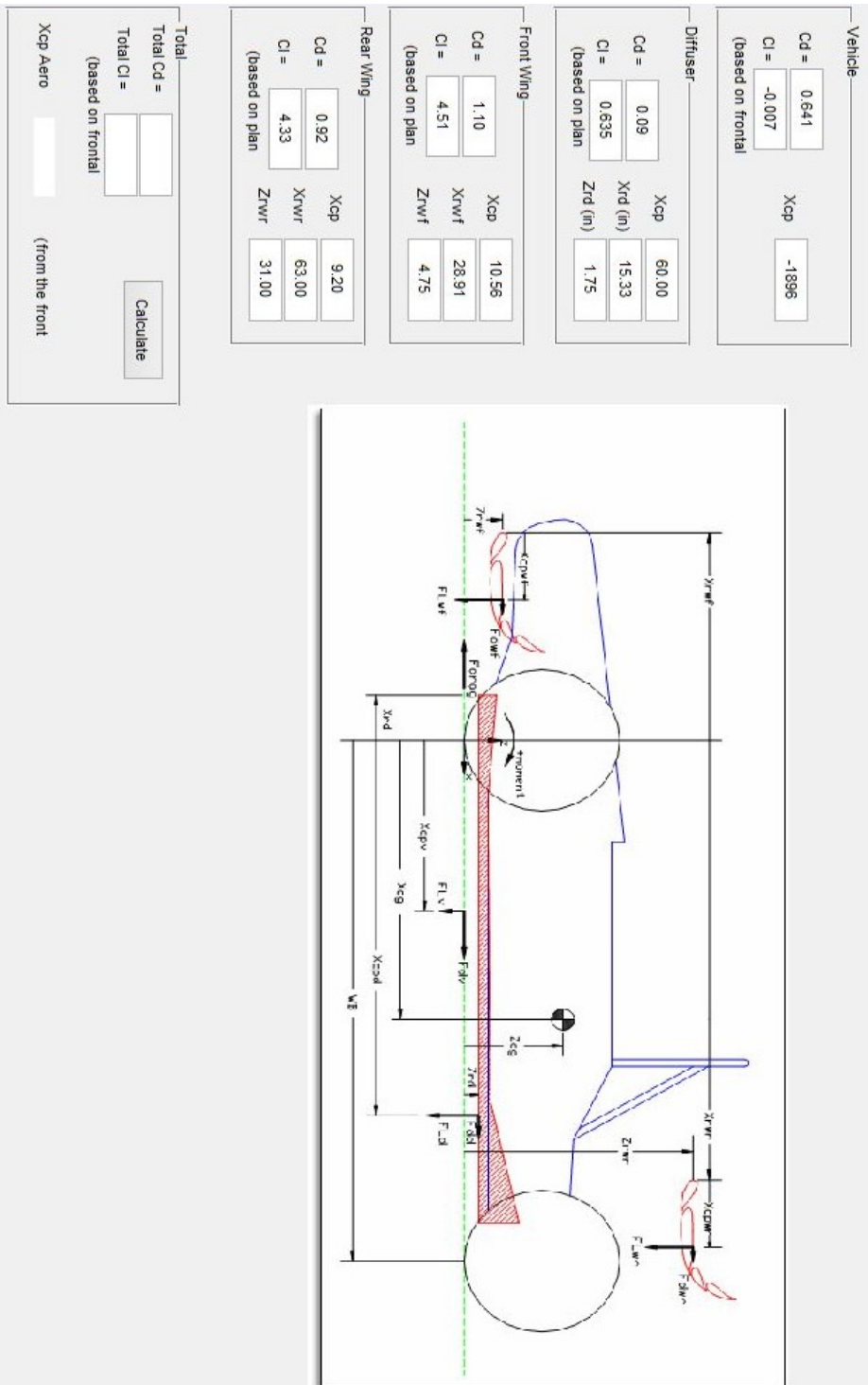
Figure 44. Module for manipulating aerodynamic data for the lap simulator.

73
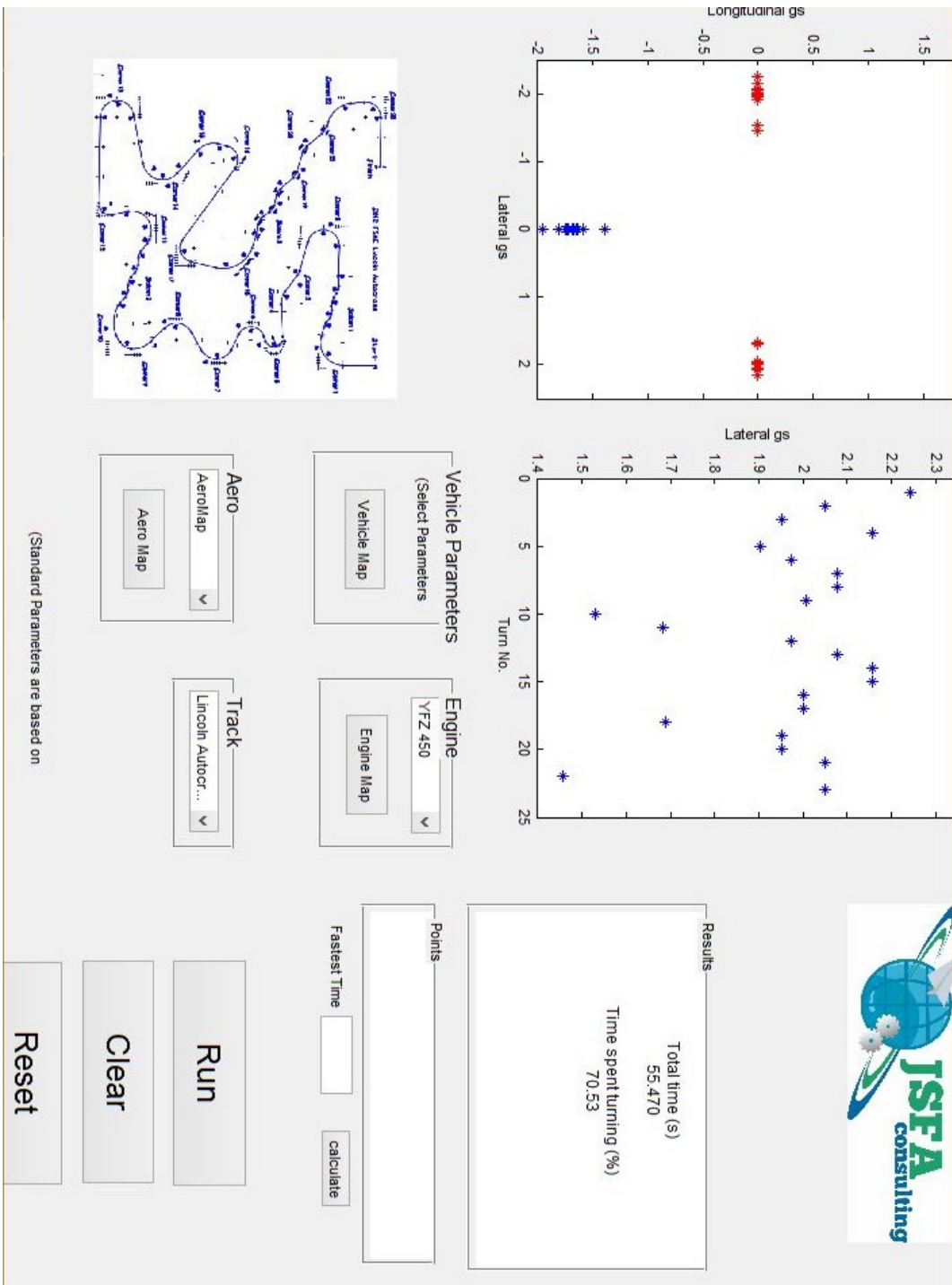
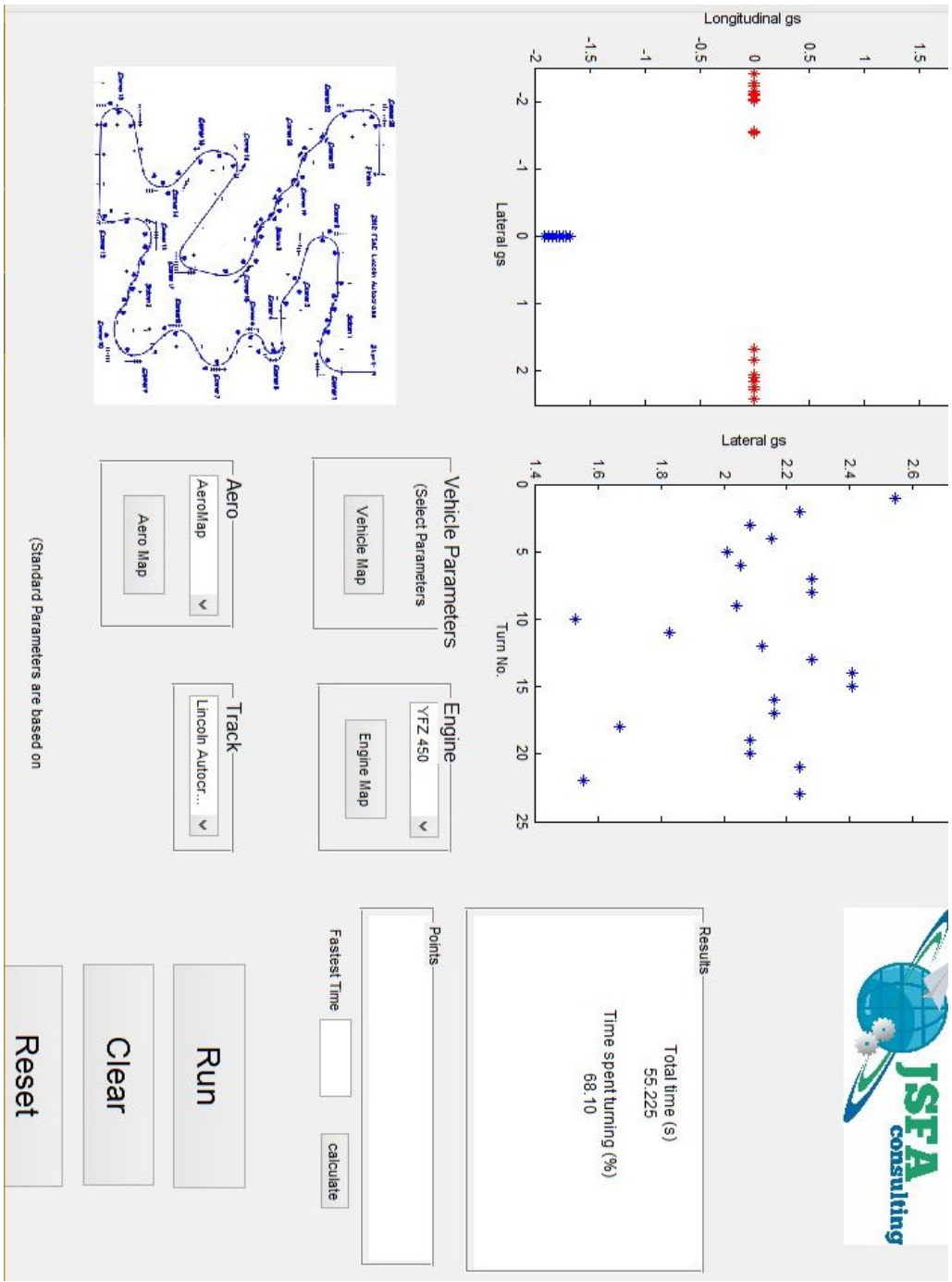Figure 45. Four-Element Static Simulation Results.

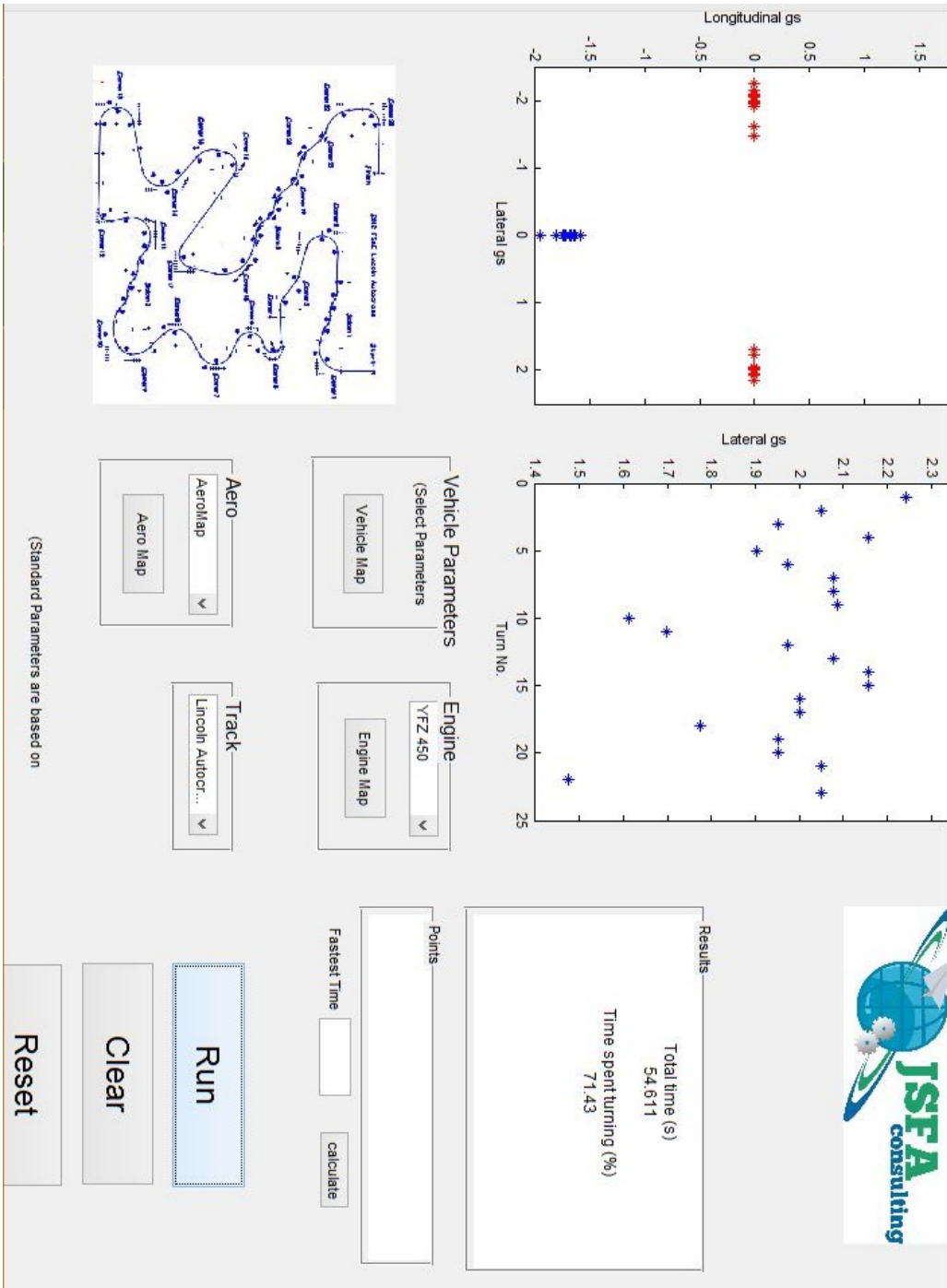Figure 46. Five-element static simulation results.
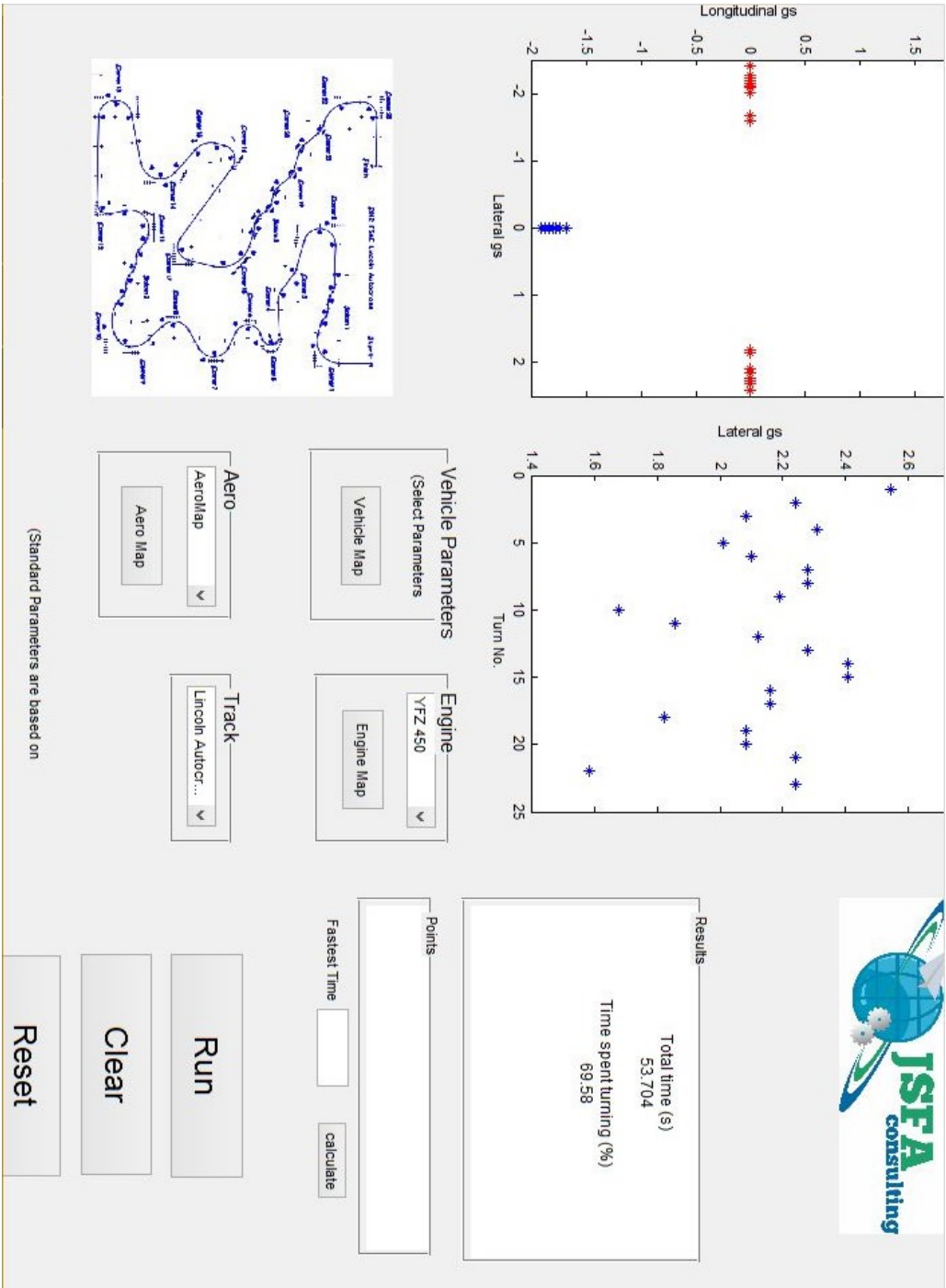
Figure 47. Four-element active simulation results.

Figure 48. Five-element active simulation results.

Appendix C

Derivation of the Line of Pressure for a Multi-Element Wing

The location of the line of pressure on a flap in a multi element wing is calculated based on the aerodynamic forces produced on the element itself. The procedure will be demonstrated on a basic dual element wing using multiple reference frames to simplify the calculation.

From the CFD simulation, the lift, drag, and moment about the origin of the main plane are given. These components are resolved in the reference frame of the wing, *[W]* shown in figure 49.
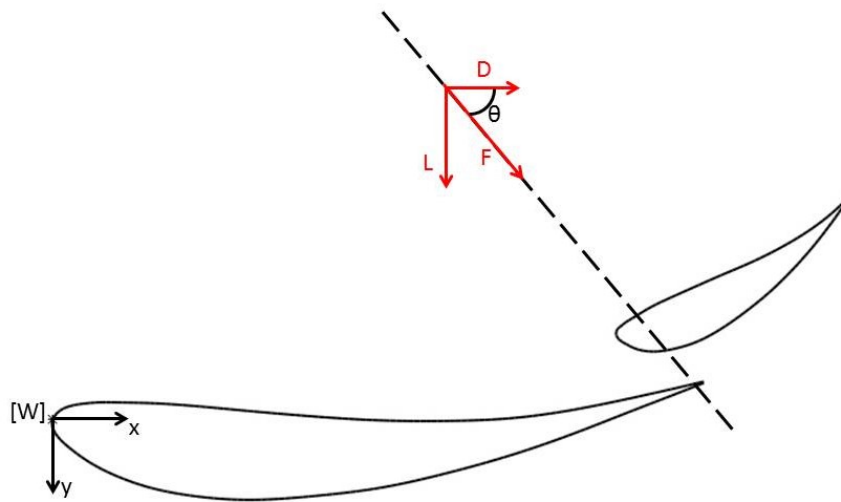

Figure 49. Resolving resultant force, F, in the [W] frame.

The resultant force vector and its angle relative to the wing frame are given by equations C.1 and C.2 respectively.

$$F = \sqrt{L^2 + D^2} \qquad\qquad \text{C.1}$$

$$\theta = \tan^{-1}\left(\frac{L}{D}\right) \qquad\qquad \text{C.2}$$

Next, we define a new reference frame *[W']* that will be used to calculate the position of the line of pressure from the origin of the main plane. This is done by rotating the wing frame, *[W]* by the angle of the resultant force theta given in the previous equation as shown in figure 4.
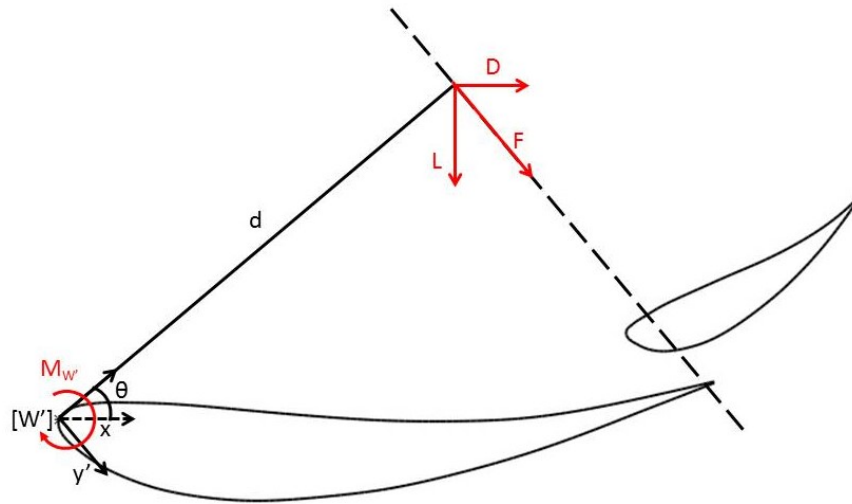
Figure 50. Position of the line of pressure in the [W'] frame.

. This gives the y-axis parallel with the resultant aerodynamic force. Therefore the moment about the origin of the [W'] frame is simply the cross product of the aerodynamic force _F_ and its distance _d_. This gives the position of the line of pressure with respect to the [W'] frame.

$$M_{\dot{W}} = r \, X \, F = \begin{bmatrix} x' \\ 0 \end{bmatrix} X \begin{bmatrix} 0 \\ F \end{bmatrix}$$ 3.3

Next we define a third reference frame [F'] centered at the leading edge of the flap. It too is rotated by angle theta so that its axes are only a translation of the [W'] frame. The pivot location will be referenced to the individual so it is pertinent to resolve the moment of the resultant force about this origin. Frame [F'] is shown in figure 51.
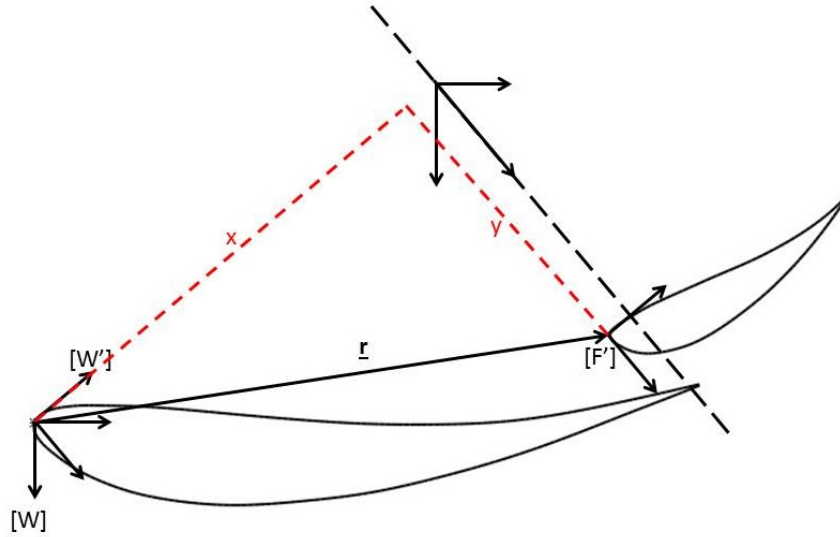
Figure 51. Position of the flap frame *[F']* with respect to the *[W']* frame.

The position of the flap frame *[F']* is given by a position vector r written in the *[W]* frame. This is the coordinate location of the leading edge of the flap relative to the leading edge of the main plane as defined by the wing design. If we write the position vector r in the *[W']* frame, we simply take its position in the *[W]* frame and multiply by a rotation matrix to get the position of the flap in the *[W']* frame.

$$\begin{bmatrix} x_F \\ y_F \end{bmatrix}_{\acute{W}} = R_{\acute{W}W} \begin{bmatrix} x_F \\ y_F \end{bmatrix}_W \qquad \text{C.4}$$

$$R_{\acute{W}W} = \begin{bmatrix} \cos\theta & \sin\theta \\ -\sin\theta & \cos\theta \end{bmatrix} \qquad \text{C.5}$$

Now we examine the location of the pivot point P on the flap. For convenience, we establish a 4th reference frame *[F]*. Its origin is located at the same point as frame *[F']* but is rotated from the wing frame *[W]* by the angle of attack of the flap, alpha. This makes the x-axis collinear with the chord of the flap. This is shown below in figure 52. Frame *[F']* from figure 51 has been removed for clarity.
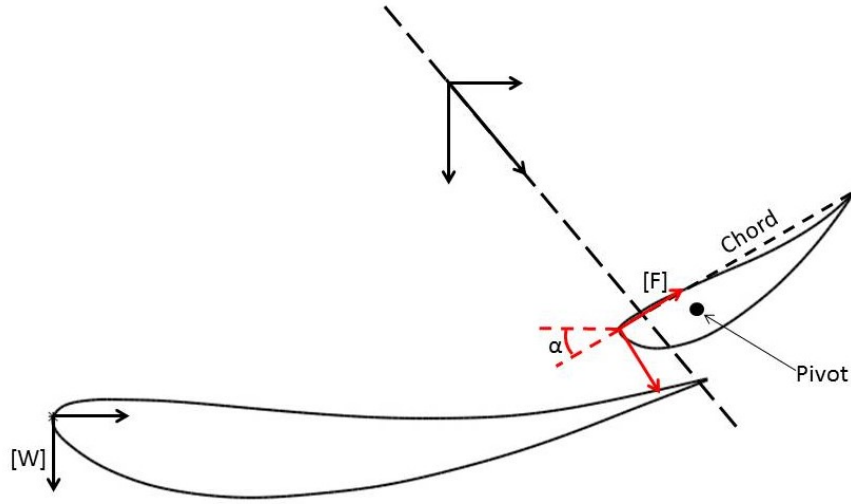
Figure 52. Position of the flap pivot with respect to the *[F]* frame.

The pivot point has coordinates x_p and y_p which then need to be defined in the *[F']* frame. For this a second rotation matrix is used to orient the position vector of the point with respect frame *[F]*. The angle of rotation is given by the angle of the line of pressure, theta, minus the angle of attack, alpha. This is shown in equations (C.6) and (C.7).

$$\begin{bmatrix} x_P \\ y_P \end{bmatrix}_{\acute{F}} = R_{\acute{F}F} \begin{bmatrix} x_P \\ y_P \end{bmatrix}_{F} \qquad\qquad \text{C.6}$$

$$R_{\acute{F}F} = \begin{bmatrix} \cos(\theta - \alpha) & \sin(\theta - \alpha) \\ -\sin(\theta - \alpha) & \cos(\theta - \alpha) \end{bmatrix} \qquad\qquad \text{C.7}$$

In order to calculate the moment about the pivot point we need the distance of the resultant aerodynamic force F to the pivot location. This is found by summation of position vectors in the *[W']* and *[F']* frames given by equations (C.3), (C.4), and (C.6). The subscript outside of the column matrices give the reference frame each vector is written in.

$$d_{\acute{F}} = R_{\acute{F}F} \begin{bmatrix} x_P \\ y_P \end{bmatrix}_{F} + R_{\acute{W}W} \begin{bmatrix} x_F \\ y_F \end{bmatrix}_{W} + \begin{bmatrix} x' \\ 0 \end{bmatrix}_{\acute{W}} \qquad\qquad \text{C.8}$$

Lastly, to calculate the moment about the pivot location point P, we cross both sides of equation (C.8) by the resultant aerodynamic force $\underline{F}$. This gives the moment about pivot point in the *[F']* frame.

$$M_{\acute{F}} = \underline{d_{\acute{F}}} \, X \, \underline{F} = \left(R_{\acute{F}F} \begin{bmatrix} x_P \\ y_P \end{bmatrix}_F + R_{\acute{W}W} \begin{bmatrix} x_F \\ y_F \end{bmatrix}_W - \begin{bmatrix} x' \\ 0 \end{bmatrix}_{\acute{W}} \right) X \begin{bmatrix} 0 \\ -F \end{bmatrix} \qquad 3.9$$

Since all the vectors are now defined in the *[W']* and *[F']* frames, the y-axis is collinear

with the aerodynamic force *F*, performing the cross product operation yields equation (C.10)

which calculates the moment about the pivot location. The first two terms give the location of the

pivot point with respect to the flap, the second two terms give the location of the flap with

respect to the leading edge of the main, and the last term gives the location of the line of

pressure with respect to the leading edge of the main.

$$M_{Pivot} = F \left(x_p \cos(\theta - \alpha) + y_p \sin(\theta - \alpha) + x_B \cos\theta + y_B \sin\theta - \frac{M_W}{F} \right) \qquad 3.10$$

Appendix D

Linkage Kinematic Equations

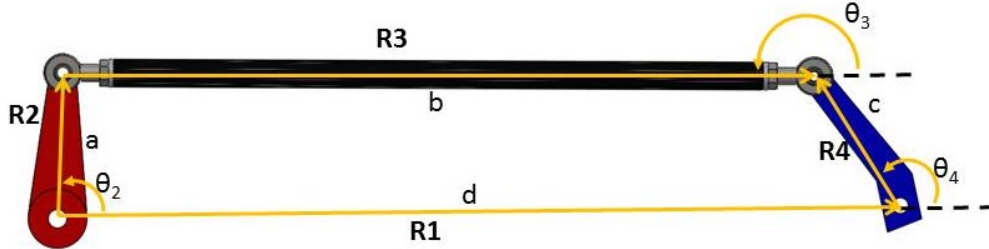Figure 53 shows the linkage with all relevant nomenclature.

Figure 53. Four bar linkage used to actuate a flap.

From equation (5.1), we substitute the cartesian expressions for each vector. Further

splitting the expression into X and Y components yields the following equations written in terms

of the link lengths, and their angular positions.

$$a\cos\theta_2 + b\cos\theta_3 - c\cos\theta_4 - d\cos\theta_1 = 0 \qquad \text{D.2}$$

$$ja\sin\theta_2 + jb\sin\theta_3 - jc\sin\theta_4 - jd\sin\theta_1 = 0 \qquad \text{D.3}$$

Equations (D.2) and (D.3) are solved simultaneously which yields the expressions for

θ_3 and θ_4 which is the output angle of the linkage.

$$\theta_3 = 2\arctan\left(\frac{-E \pm \sqrt{E^2 - 4DF}}{2D}\right) \qquad \text{D.4}$$

$$\theta_4 = 2\arctan\left(\frac{-B \pm \sqrt{B^2 - 4AC}}{2A}\right) \qquad \text{D.5}$$

With:
$A = \cos\theta_2 - K_1 - K_2\cos\theta_2 + K_3$ D.6
$B = -\sin\theta_2$ D.7
$C = K_1 - (K_2 + 1)\cos\theta_2 + K_3$ D.8
$D = \cos\theta_2 - K_1 - K_4\cos\theta_2 + K_5$ D.9
$E = -2\sin\theta_2$ D.10
$F = K_1 - (K_4 + 1)\cos\theta_2 + K_5$ D.11

$$K_1 = \frac{d}{a} \qquad \text{D.12}$$

$$K_2 = \frac{d}{c} \qquad \text{D.13}$$

$$K_3 = \frac{a^2 - b^2 + c^2 + d^2}{2ac} \qquad \text{D.14}$$

$$K_4 = \frac{d}{b}$$ D.15

$$K_5 = \frac{c^2 - d^2 - a^2 - b^2}{2ab}$$ D.16

Equations (D.4) – (D.16) above are then solved for each of the three flap mechanisms. Link a is the input link at the servo, link b is the push/pull rod connecting the servo to the flap, link c is the lever arm at the wing element and link d is the distance between the pivot locations.

Once the position analysis of the linkage is calculated, the mechanical advantage and velocity ratios can be calculate using equations (D.17 – D.20) [13].

$$m_v = \frac{a sin\alpha}{c sin\beta}$$ D.17

$$m_v = \frac{a sin\alpha}{c sin\beta}$$ D.18

$$\alpha = \theta_2 - \theta_3$$ D.19

$$\beta = \theta_4 - \theta_3$$ D.20

Appendix E

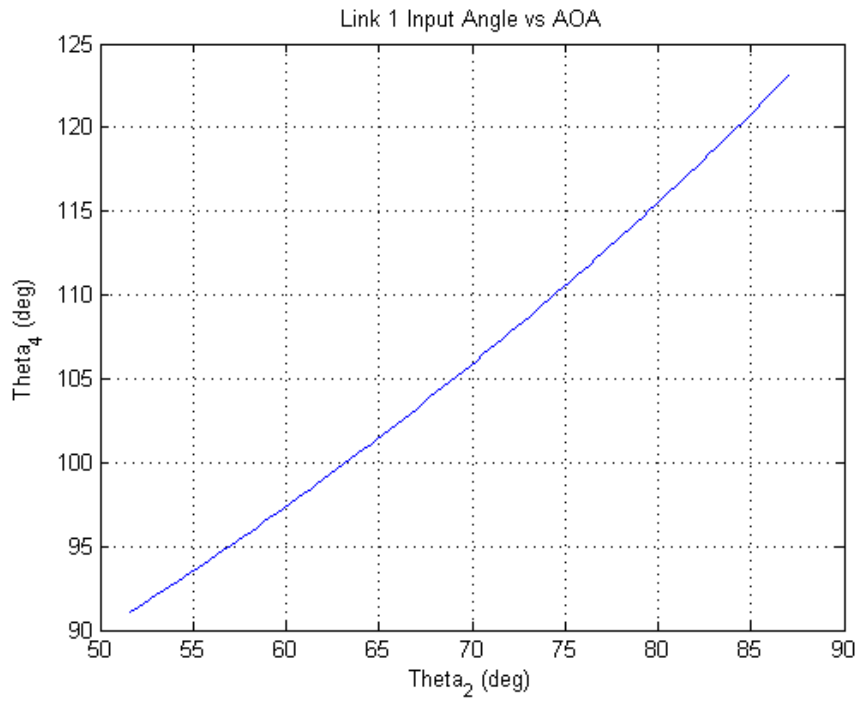Linkage Position, Mechanical Advantage, and Velocity Ratios

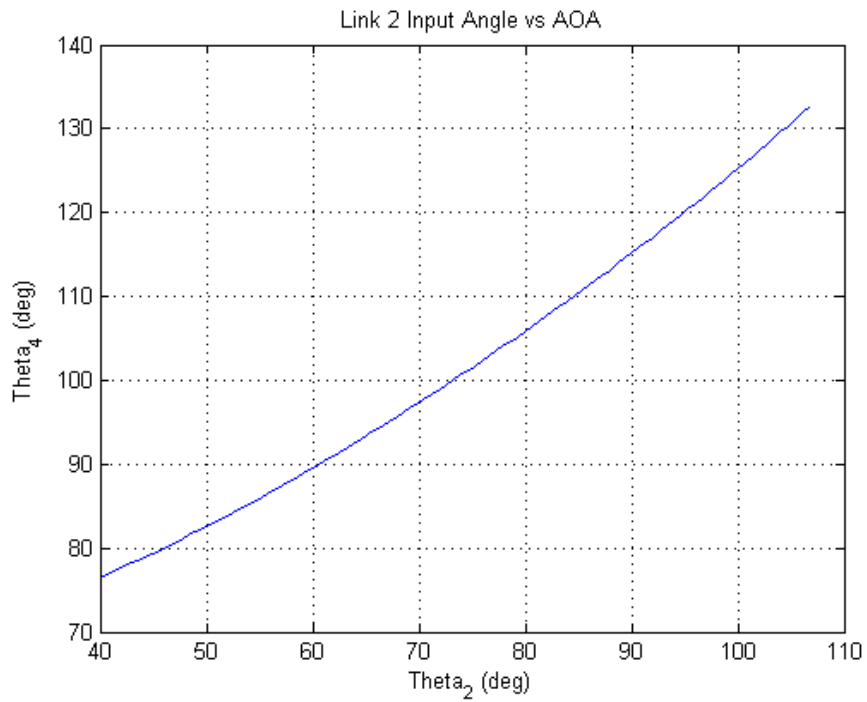Figure 54. Input angle vs AOA for link 1.
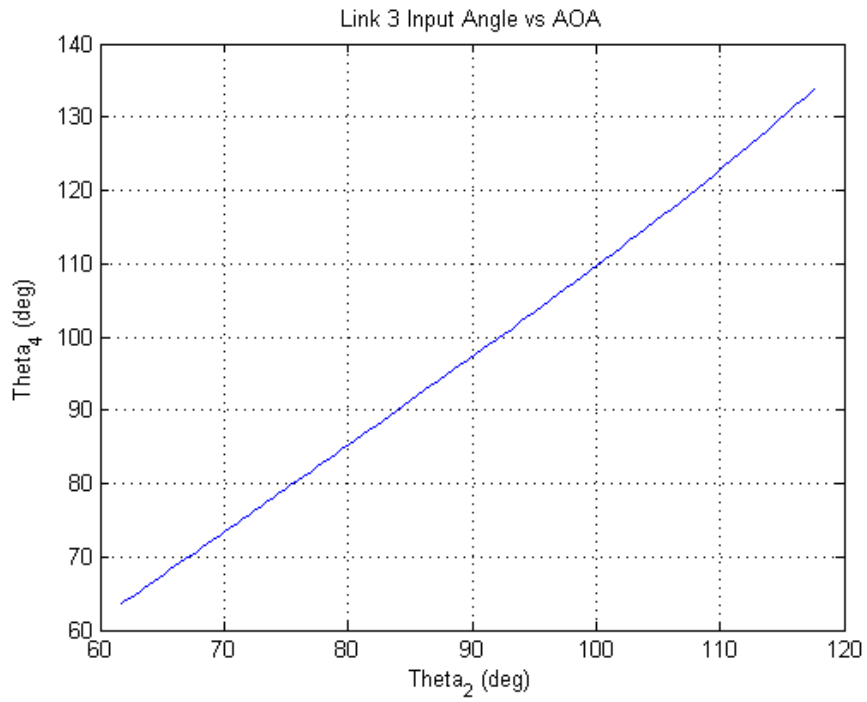

Figure 55. Input angle vs AOA for link 2.
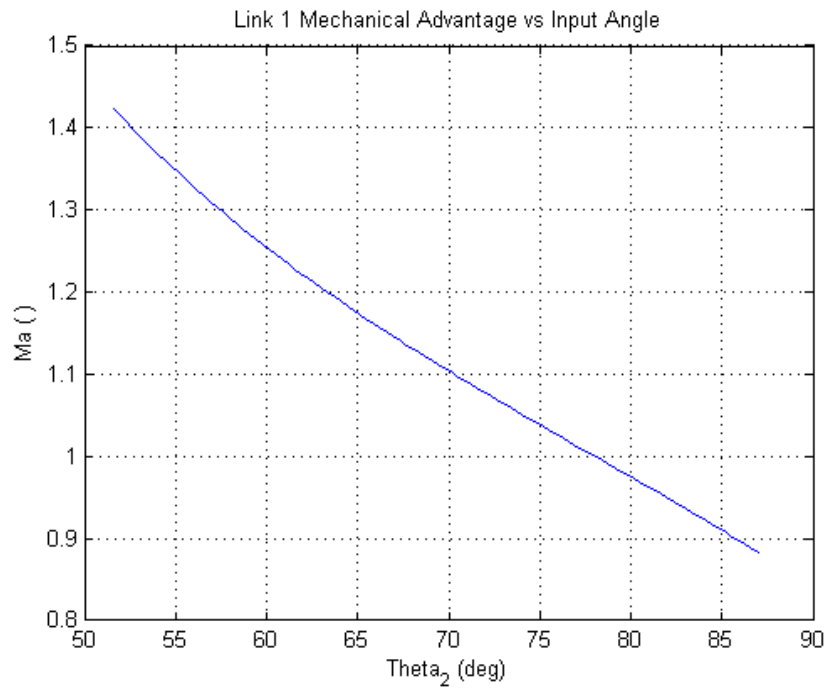
Figure 56. Input angle vs AOA for link 3.

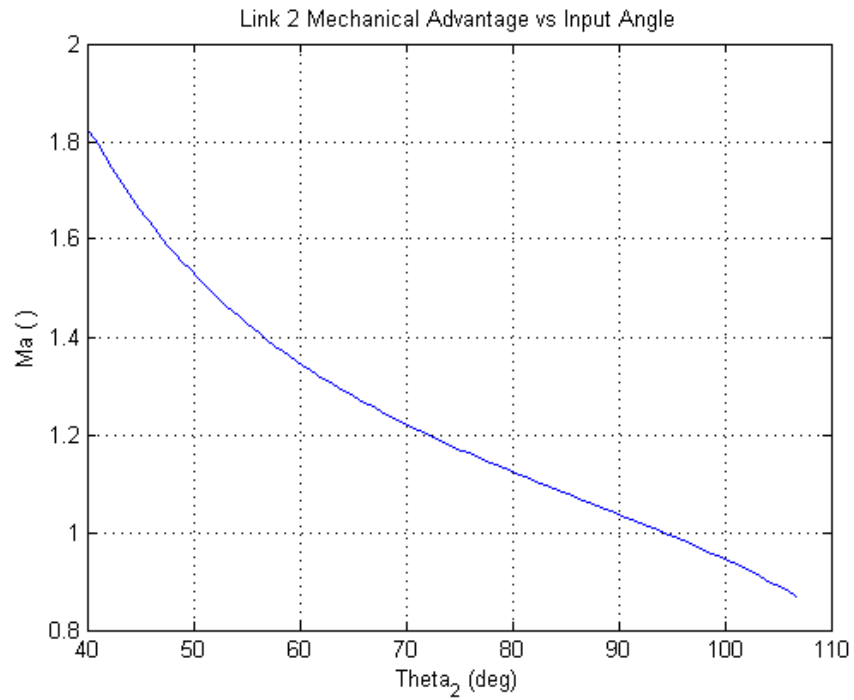Figure 57. Mechanical advantage vs input angle for link 1.

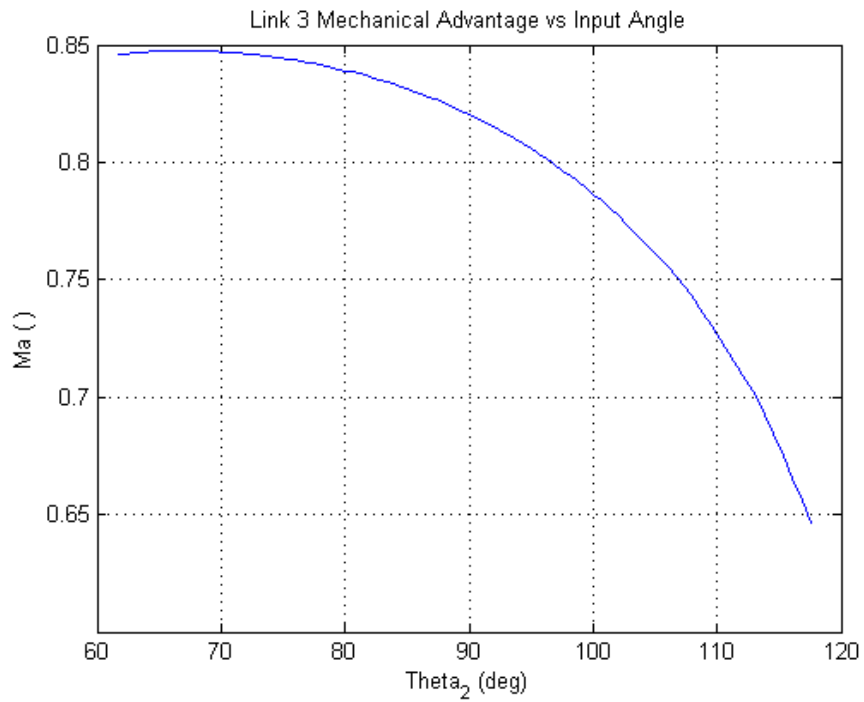Figure 58. Mechanical advantage vs input angle for link 2.

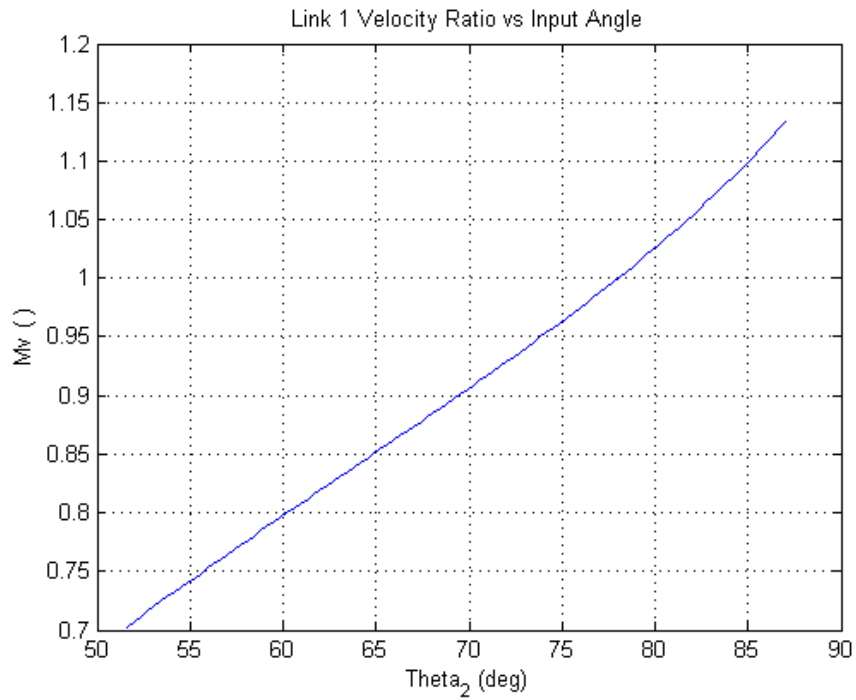Figure 59. Mechanical advantage vs input angle for link 3.

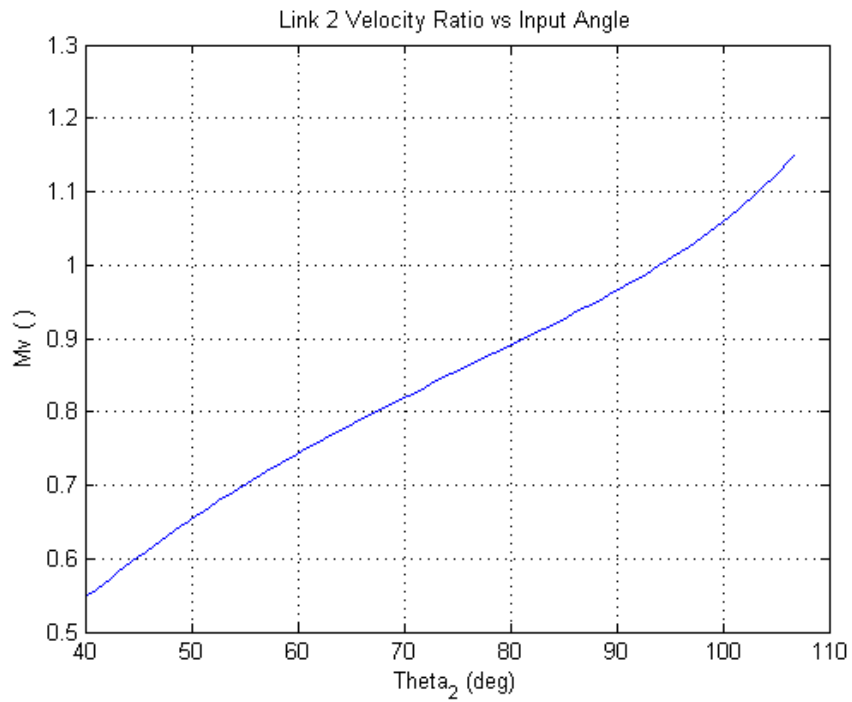Figure 60. Velocity ratio vs input angle for link 1.

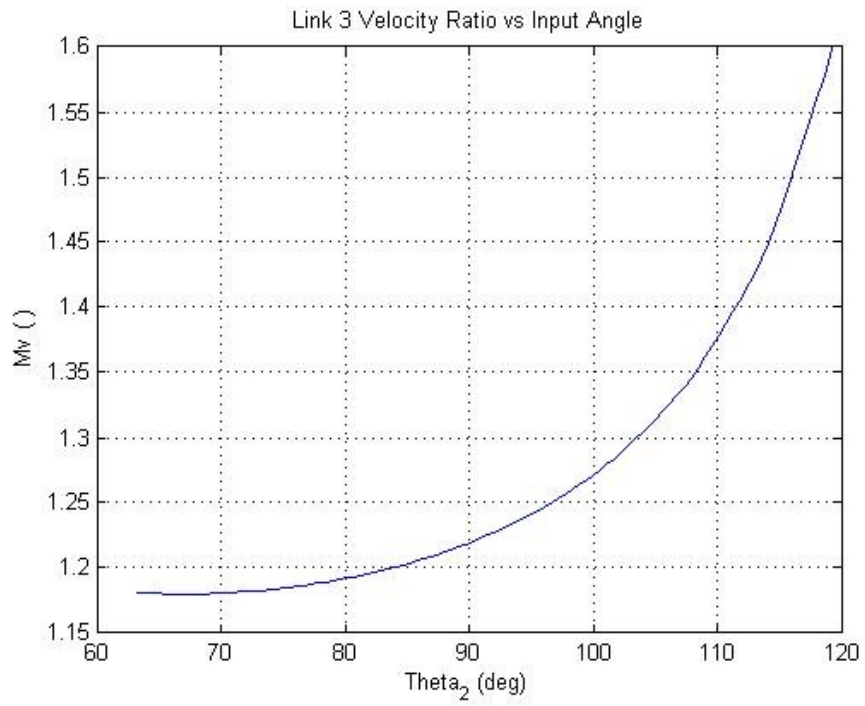Figure 61. Velocity ratio vs input angle for flap 2.

Figure 62. Velocity ratio vs input angle for flap 3.

Appendix F

Itemized Component Weights

Table 13. Itemized component weights

Part	Number	Weight			
Bearing Cups	24	2.74	[g]	0.14	[lb]
Lim-Switch Insert	16	0.53	[g]	0.02	[lb]
Linkage Tube	24	0.5	[g]	0.03	[lb]
Servos	8	56	[g]	0.99	[lb]
Servo Arms	16	7	[g]	0.25	[lb]
Endcap Arms	8	3	[g]	0.05	[lb]
Limit switches	8	2	[g]	0.04	[lb]
Bearings	24	3	[g]	0.16	[lb]
Linkage tubing	2	30	[g]	0.13	[lb]
Rod Ends	24	1	[g]	0.05	[lb]
AAC Box	1	650	[g]	1.43	[lb]
Wiring [in]	60.83	0.6	[g]	0.08	[lb]
Connectors	8	5	[g]	0.09	[lb]
Heat Shrink [in]	30.42	3	[g]	0.20	[lb]

	Total:	764.37	[g]	3.66	[lb]

References

1. 2012 Endurance Data. July 2012. Raw data. FSAE archived data.

2. Attravanam, Siddarth K. Laptime Simulation and Path Optimization. Thesis. University
   of Texas at Arlington, 2012. Print.

3. Chaparral Official Web Site. 2005. Web. http://www.chaparralcars.com/index.ph

4. Formula SAE Lincoln 2012 Overall Results. July 2012. Raw data.
   Http://students.sae.org/competitions/formulaseries/results/, Lincoln, Nebraska.

5. 2013 Formula SAE Rules. SAE International. Online.
   http://students.sae.org/cds/formulaseries/rules/2013fsaerules.pdf

6. Fung, Y. C. An introduction to the Theory of Aeroelasticity. Mineola: Dover, 1993. Print.

7. Katz, Joseph. Race Car Aerodynamics: Designing for Speed. Cambridge: Bentley,
   2006. Print.

8. Long, Aaron. "Developments in Low Speed Aerodynamics for the 2012 Formula SAE
   Car." Pointwise User Group Meeting. Fort Worth. 2011.

9. Long, Randy. Hibbard, Michael. Rivas, Naima. "Preliminary Technical Report on the
   UTA FSAE Active Aero Computer" 2013. Print.

10. McBeath, Simon. Competition Car Aerodynamics: A Practical Handbook. Newbury
    Park: Haynes, 2006. Print.

11. Merkel, James P. "Aeroelastic Analysis of Active Aerodynamics". 2013. Print.

12. Merkel, James P. "Rolling Resistance of the Formula SAE Car". 2012. Print

13. Norton, Robert L. Design of Machinery: An Introduction to the Synthesis and Analysis
    of Mechanisms and Machines. 4th ed. New York: McGraw-Hill College, 2008.
    Print.

14. Woods, Robert L., and Kent L. Lawrence. Modeling and Simulation of Dynamic
    Systems. Upper Saddle River, NJ: Prentice Hall, 1997. Print.

Biographical Information

James Merkel was born March 17, 1989 in Garland, Texas. He is the oldest of the six children of Jim and Debbie Merkel. He started attending the University of Texas at Arlington in the fall of 2007 pursuing a double major in Mechanical and Aerospace Engineering. He graduated in spring of 2012 and started working on a Masters in Aerospace Engineering in the fall of that year. James received his graduate degree in December of 2013.

He officially joined the Formula SAE team fall of 2008 and worked with them throughout both his undergraduate and graduate career. During his tenure he has focused on vehicle aerodynamics and wing design for the cars. This includes the design of a clean sheet multi element wing that is currently in use on both the front and rear of the car. He has also served as the Team Captain, and Chief Engineer for various cars.